Functionalization of Carbon-Carbon Multiple Bonds by High Oxidation State Chemical Species

（高酸化度化学種を利用した炭素－炭素不飽和結合の修飾）

Emna MEJRI

2023

Contents

Chapter 1

General Introduction

Overview

Carbon-Carbon (C-C) multiple bonds, serving as the cornerstone of many organic compounds extracted from petroleum resources and obtained from natural origins, act as key site for functional group attachment, thereby enabling the evolution of base molecules into value-added, complex chemical structures.

This bond serves as a fertile platform for functional group introduction, facilitating the transformation of base molecules into more complex structures with considerably higher value. Carbon-Carbon multiple bonds exhibit inherent nucleophilic characteristics primarily due to their rich electron density. This unique property makes them particularly attractive in organic synthesis as they are amenable to modifications through a diverse array of reactions with electrophilic counterparts. The hydration reaction, carried out in acidic aqueous solutions such as sulfuric acid, stands as a classic example of the potential for multiple bond modification.

Harnessing the reactivity of C-C multiple bonds for functionalization necessitates the creation of highly electrophilic active species. One prevalent strategy to achieve this involves the employment of high oxidation state chemical species. Such chemical species are inherently electron-deficient due to their high oxidation state, thereby exhibiting enhanced electrophilicity. This characteristic makes them ideal for initiating reactions with electron-rich C-C multiple bonds.

The use of high oxidation state chemical species, hence, presents a compelling route to the functionalization of C-C multiple bonds. I delve into this topic further by categorizing these reactions into two primary types: those catalyzed by transition metals and those involving non-metallic chemical species. In the sections that follow, these reactions will be analyzed, aiming to uncover the full potential of C-C multiple bond modification reactions using high oxidation state chemical species.

1. Functionalization of C-C multiple bonds

1.1 Functionalization of C-C multiple bonds using high oxidation state transition metal catalysts :

The oxidation state of metal complexes provides a basis for comparing their electrophilicity, with higher oxidation state complexes generally considered more electrophilic. Metal complexes, as catalysts, hold great promise for the functionalization of C-C multiple bonds. According to the Hard-Soft Acid-Base (HSAB) rule, soft transition metal complexes are particularly effective for the functionalization of soft C-C multiple bonds. Consequently, numerous C-C multiple bond modification reactions utilizing soft transition metal catalysts with high oxidation states have been reported, showcasing their potential.

In recent years, significant advancements have been made in catalytic reactions involving highly active Cu(III) and Pd(IV) species, which can be regarded as high-valent metals. These high-valent metal species exhibit enhanced electrophilicity and have proven to be valuable catalysts for C-C multiple bond transformations. The progress achieved in the field of C-C bond modification using high-valent metals highlights the importance of considering both the oxidation state and the softness of the transition metal complexes in catalyst design. By leveraging the electrophilicity of high oxidation state metal complexes and the softness of transition metals, chemists have unlocked new possibilities for efficient and selective C-C multiple bond functionalization. For instance, Cu(III)-catalyzed oxidative coupling reactions have been successfully employed for the direct functionalization of C-C multiple bonds.**[1]** These reactions enable the construction of complex organic molecules with high regioselectivity and efficiency.

Gaunt's research group demonstrated a reaction involving alkenes and organocopper(III) species (Scheme 1). In this case, organocopper(III) species with high oxidation states acted as electrophiles, while alkenes served as nucleophiles. The combination of a copper catalyst and a diaryliodonium salt generated an aryl-Cu(III) intermediate, which acted as a highly activated aryl cation-like species. An alkene nucleophile attacked the aromatic electrophile, leading to the formation of a C-

C bond. Deprotonation from the generated intermediate resulted in the regeneration of a C-C double bond. **[2]**

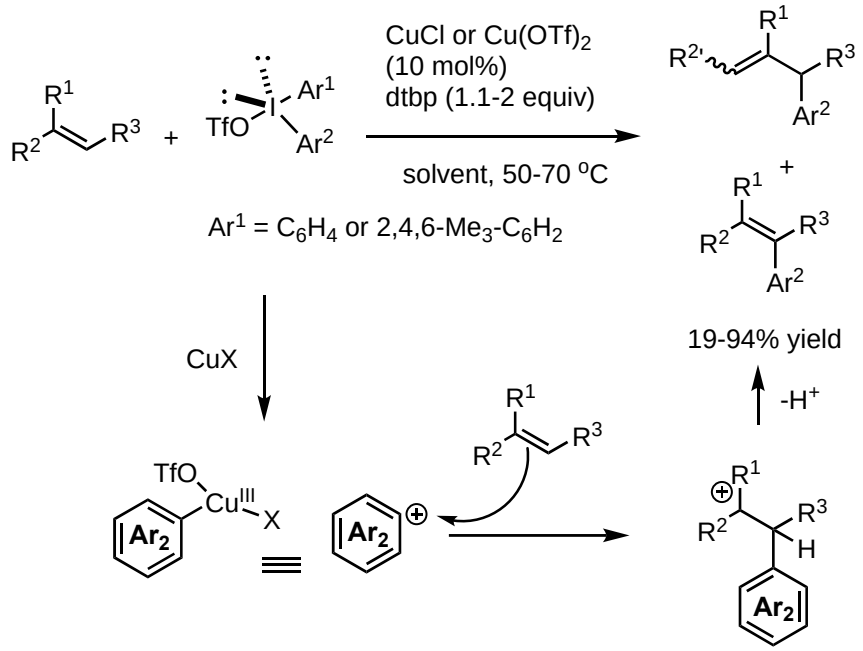

Scheme 1 : Electrophilic arylation of alkenes developed by Gaunt. (2012)

In the realm of electrophilic activation of alkynes , Gaunt's research group has developed an innovative strategy for constructing tri- or tetra-substituted alkenes through an electrophilic syn-carbotriflation of alkynes**.[3]** By employing a CuCl catalyst in conjunction with vinyl- or diaryliodonium triflates, highly electrophilic carbon species, potentially vinyl- or aryl-A-Cu(III) species, are generated. These species subsequently react with alkynes to form putative vinyl-Cu(III) intermediates (Scheme 2). Through reductive elimination from the vinyl-Cu(III) species, tri- and tetra-substituted vinyltriflates are obtained. This electrophilic carbofunctionalization approach complements the nucleometalation of alkynes and is applicable to both internal and terminal alkynes.

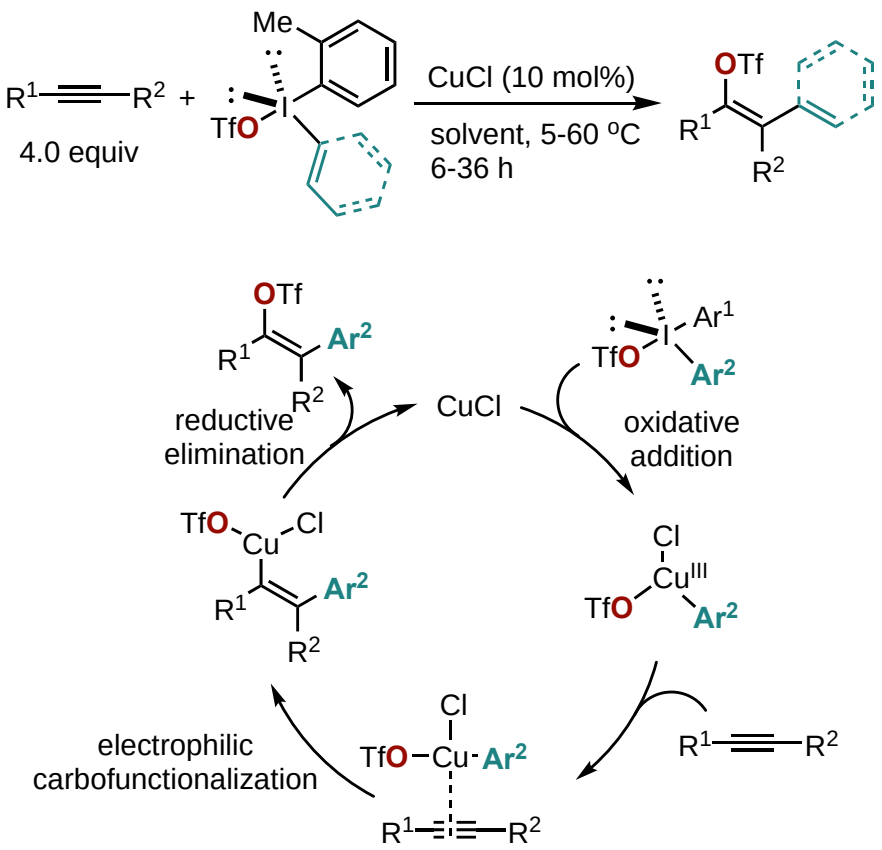

Scheme 2 : Plausible mechanism of tri- and tetra-substituted vinyltriflates synthesis developed by Gaunt. (2013)

Pd(IV) species have also emerged as powerful species for C-C multiple bond activation. Pd-catalyzed reactions involving Pd(IV) species have been utilized in various transformations, including C-H activation and oxidative coupling reactions. These reactions enable the direct functionalization of C-C multiple bonds, providing access to structurally diverse and synthetically valuable compounds.

The Sorensen group, in 2005, revealed their findings on Pd(II)-catalyzed aminoacetoxylation of alkenes ring formation via alkyl Pd(IV) as a key intermediate.**[4]** Their initial work involved the use of basic alkenyl nosylsulfonamide. In an experiment, they applied 10 mol % $Pd(OAc)_2$, adding 2.0 equivalents of $PhI(OAc)_2$ (that plays important role in oxidizing the neutral alkyl-Pd(II) intermediate into alkyl-Pd(IV) intermediate) in CH_2Cl_2 .

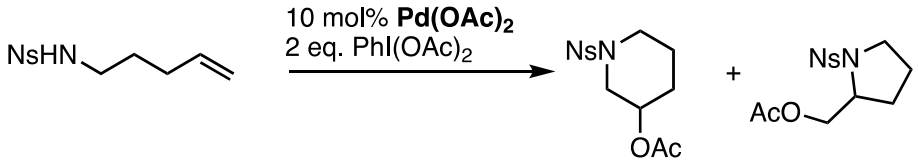

Scheme 3 : Palladium-catalyzed ring-forming aminoacetoxylation of alkenes. (2005)

Muniz's team expanded the scope by pioneering the Palladium(II)-catalyzed intramolecular diamination of unfunctionalized alkenes.**[5]** The expectation was that the palladium would be displaced by the urea's second amino group under oxidative conditions (via alkyl-Pd(IV) intermediate), reinstating the palladium(II) catalyst and liberating the diamination product as a cyclic urea. The reoxidant selection was crucial in all cases, with the hypervalent iodine reagent $PhI(OAc)_2$ proving the most efficient among those examined. Employing $Pd(OAc)_2$ as a precatalyst, and under gentle conditions (CH_2Cl_2, room temperature), the diamination process and simultaneous formation of five-, six-, and seven-membered fused rings were successfully achieved.

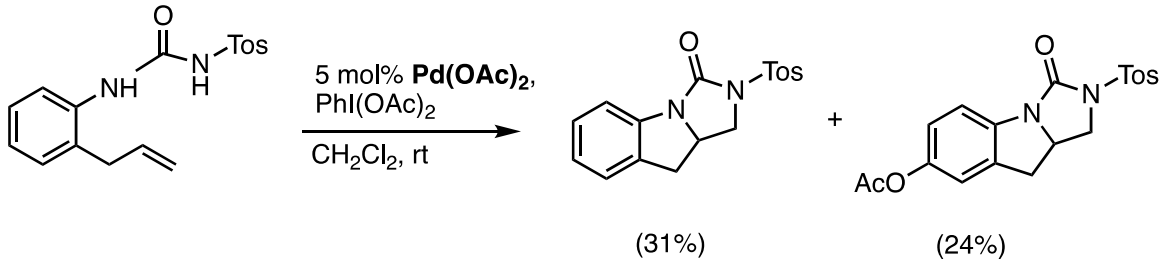

Scheme 4 : Palladium-catalyzed intramolecular diamination of alkenes. (2005)

Liu team recently delved into the palladium(II)-catalyzed oxidative difunctionalization of alkenes, employing what they termed a "high-valent palladium strategy". This strategy facilitates the production of fluorine-rich organic molecules, which are typically hard to achieve through conventional methods. By drawing on existing alkene difunctionalization methods, they were able to create a range of heterocycles that contained fluorine, trifluoromethyl, and trifluoromethoxyl groups from alkene substrates, under benign reaction conditions. In addition to hypervalent iodine reagents, electrophilic fluorinating reagents can oxidize alkyl C−Pd(II) species into high-valent alkyl C−Pd(IV) intermediates for palladium-catalyzed oxidative fluorination reactions. This

discovery paved the way for several successful catalytic difunctionalizations of alkenes, including aminofluorination,**[6]** aryltrifluoromethylation, ditrifluoromethoxylation.**[7]**

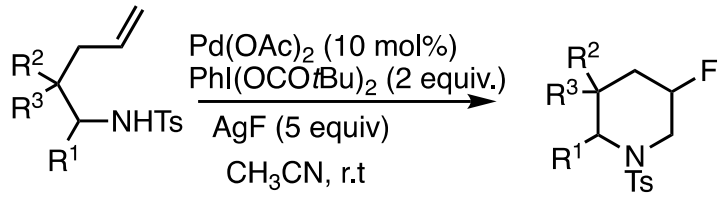

Scheme 5 : Pd(II)-catalyzed intramolecular aminofluorination of alkenes. (2016)

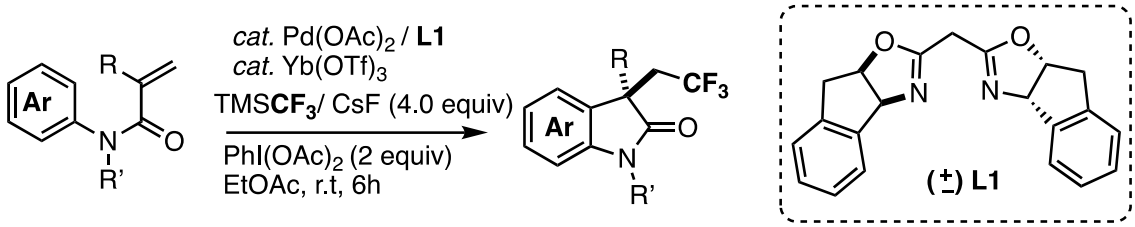

Scheme 6 : Aryltrifluoromethylation of alkenes .

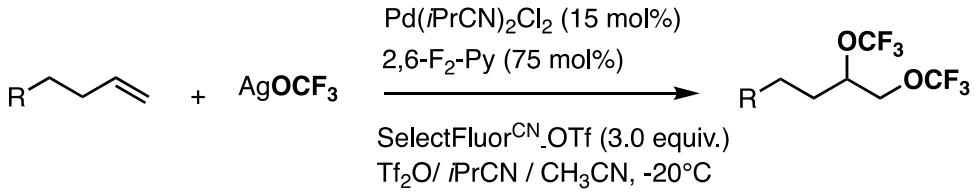

Scheme 7 : Palladium-catalyzed intermolecular ditrifluoromethoxylation of unactivated alkenes: CF_3O-palladation initiated by Pd(IV). (2018)

Functionalization of C-C multiple bonds using Au catalysts

Gold catalysts are useful for functionalizing C-C multiple bonds. While high-valent metals are valuable as active intermediates in catalytic reactions, they are difficult to isolate and modify. In contrast, Au(III), despite its high oxidation state, is stable enough to use independently as a catalyst, making it attractive for C-C multiple bond modification reactions. Due to their soft properties, Au catalysts can facilitate C-C multiple bond modification reactions even in a lower oxidation state as Au(I). This stable and easy-to-handle form has enabled the development of various reactions.

Au(I)-catalyzed C-C multiple bond functionalization:

In 2004, Toste and his team explored the efficiency of group 11 metal catalysts in the Conia-ene reaction for intramolecular addition of a β-ketoester to an unactivated alkyne. The triphenylphosphinegold(I) cation rapidly converted the starting material into the desired product at room temperature.**[8] [9]**

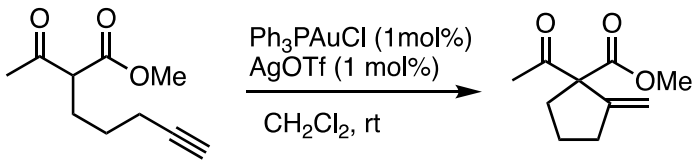

Scheme 8 : Alkyne activation through Au(I) complexes in Conia-ene reaction .

In 2013, Toste's group demonstrated the usefulness of Au(I) catalyst for the functionalization of allenes. Combined use of Au(I) catalyst with electrophilic halogen source promoted aminohalogenation of allenes.**[10]**

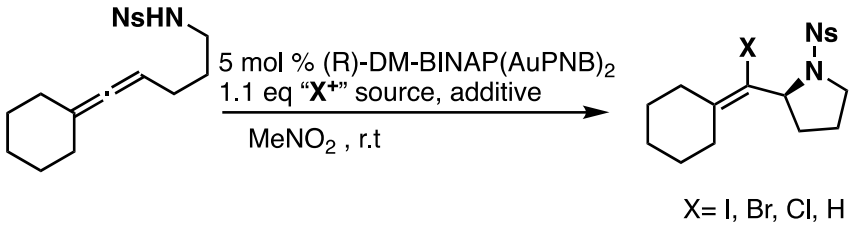

Scheme 9 : Gold(I)-catalyzed enantioselective aminohalogenation of allenes. (2013)

Au(III)-catalyzed C-C multiple bond functionalization:

The passage highlights the prospects of using gold in a higher oxidation state (Au(III)) in catalysis. This is anticipated to yield a more diverse and active catalytic system than the one using the lower oxidation state Au(I). In addition, the square planar structure of the Au(III) complex, in comparison to the linear Au(I) complex, allows ligands to be closer to the catalytic reaction field. This proximity could give ligands more influence over the reaction, thereby offering more precise control over the catalytic reaction design. Hence, Toste's group developed chiral Au(III)-catalyzed enantioconvergent 1,5-enyne cycloisomerization. Their original chiral NHC-Au(III) complex was quite effective to realize the kinetic resolution.

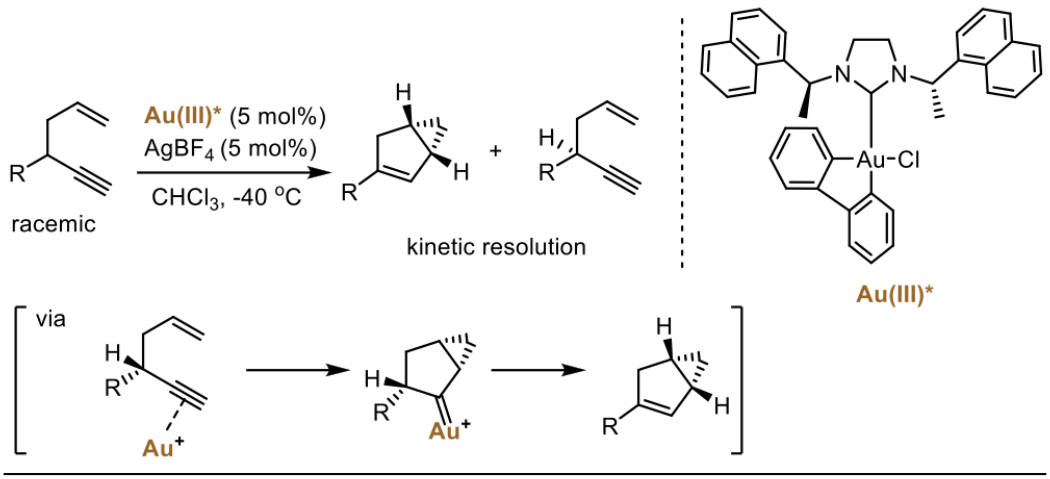

Scheme 10 : Gold(III)-catalyzed enantioconvergent 1,5-enyne cycloisomerization.

Despite the potential of Au(III) complex for catalytic functionalization of C-C multiple bonds, structural diversity of Au(III) is rather limited due to the lack of convenient method for Au(III) complex synthesis.

1.2 Functionalization of C-C multiple bonds using high oxidation state non-metallic chemical species:

Non-metallic chemical species have also been employed in C-C multiple bond modification reactions. For instance, the use of hypervalent iodine reagents offer an alternative to transition metal catalysts and have found utility in various synthetic applications.

Since the early 2000s, hypervalent iodine chemistry has seen vast advancement, with numerous organic synthesis applications owing to its air and moisture stability, accessibility, low toxicity, and user-friendly handling under mild conditions. Crucially, its unique oxidizing capability compared to transition metals has led to its increased study and use in synthetic organic chemistry. **[11]**

The first effective stereoselective oxyaminations is presented taking advantage of high electrophilicity of chiral hypervalent iodine compounds. **[12]** Introducing tert-butyldimethylsilyl

triflate (TBDMSOTf) or trimethylsilyl triflate (TMSOTf) to (diacetoxyiodo)benzene created the more reactive $PhI(OTf)_2$ in situ. This accelerated the reaction, generating bicylic products in 3 h.

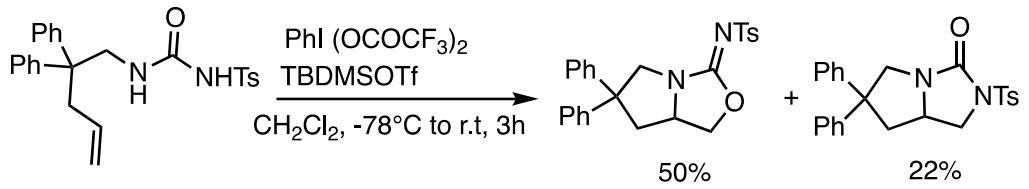

Scheme 11 : Highly stereoselective metal-free oxyaminations using chiral hypervalent iodine reagents. (2012)

Hypervalent iodine reagents are also effective for aminohalogenation reactions. Zhang's team reported the inaugural metal-free intramolecular aminofluorination of homoallylamine, employing PhIO as the oxidant and $BF_3{\cdot}OEt_2$ as the fluorine source.**[13]** A more pragmatic approach was introduced by Kitamura and colleagues,**[14]** who developed both stoichiometric methods using a PIDA/HF combination, and a catalytic method utilizing *p*-iodotoluene/mCPBA for the synthesis of 3-fluoropyrrolidines. More recently, Jacobsen et al. demonstrated the synthesis of *syn*-beta-fluoroaziridine through intramolecular aminofluorination of allylic amine using dibenzyl lactate-based chiral hypervalent iodine.**[15].**

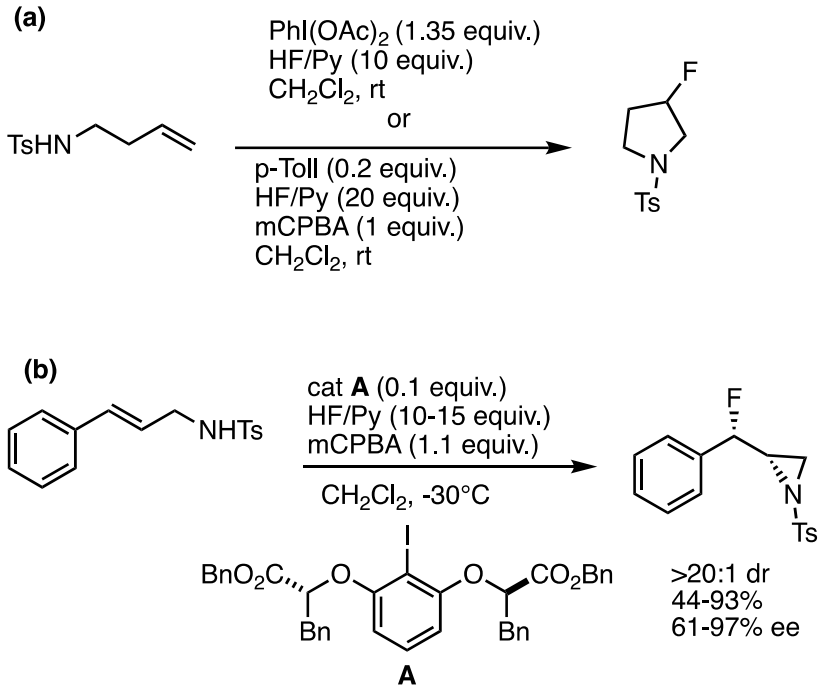

Scheme 12: (a) Aminofluorination of homoallylamine and (b) catalytic enantioselective aminofluorination.

1.3 Functionalization of C-C multiple bonds via photoinduced homolytic cleavage of the bond between heteroatoms :

Highly reactive substances, such as hypervalent iodine compounds, are versatile in numerous reactions but their requirement in more than stoichiometric quantities can lead to functional group compatibility issues. On the other hand, if a small quantity of reactive species can be generated from a stable molecule via external stimuli, side reactions can be minimized and functional group tolerance would be enhanced. One advancement in this regard involves generating electrophilic radicals through homolytic cleavage of a bond between heteroatoms using visible light energy. This cleavage generates two radicals, with one attaining a higher oxidation state, becoming highly electrophilic, and reacting swiftly with electron-rich C-C multiple bonds.

In 2021, Glorius and his colleagues proposed a metal-free photosensitization method for integrating both amine and alcohol functionalities into alkene sources in one step using thioxanthone as photocatalyst. Their approach involved using oxime carbonate as a bifunctional source of O- and N-radicals for the vicinal oxyimination of unactivated alkenes via radical–radical cross-coupling.**[16].** The homolytic cleavage of N-O bond increased the oxidation state of O atom, and the generated O-radical shows high electrophilicity to promote C-O bond formation with electron-rich alkenes. Thus generated carbon radical reacts with N-radical to furnish oxyamination of the alkenes. Similar approach was also effective for carboimination of alkenes.

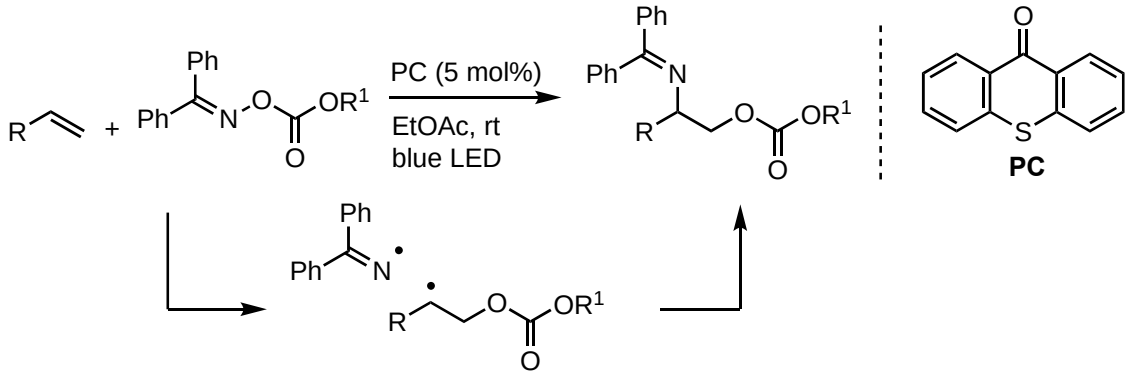

Scheme 13 : Introduction of oxime carbonate as a bifunctional O- and N-radical source for vicinal oxyimination of unactivated alkenes through radical–radical cross-coupling . (2021)

In the same year, Huo group presented an intermolecular vicinal O−N difunctionalization of olefins using oxime esters through energy transfer iridium catalysis. **[17]**

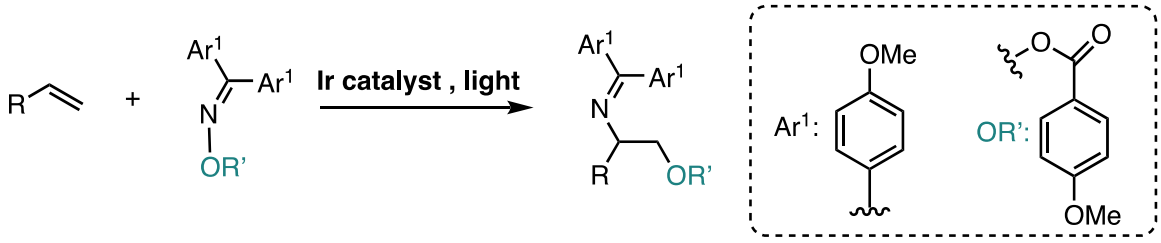

Scheme 12: Visible-light-induced intermolecular oxyimination of alkenes.

Overview of This Thesis

I have developed a series of protocols for C-C multiple bond functionalization using high oxidation species.

Chapter 2 details the Gold(III)-catalyzed multiple bond functionalization via C,N,N-cyclometalated Au(III) complexes. Meanwhile, Chapter 3 illustrates a catalyst-free approach to aminochlorination of alkenes activated by visible light.

Chapter 2 : Au(III)-Catalyzed C-C Multiple Bond Functionalization

I synthesized a series of neutral C,N,N Au(III) complexes with *N*- (8-quinolinyl)benzamide derivatives and chiral *N*-(2-(oxazolin-2-yl)phenyl)benzamide derivatives. This convenient synthesis method for amide ligands as well as an operationally simple complexation by direct C-H auration permitted changes to both the steric and electronic properties of the Au(III) complexes was tested to promote the catalytic three-component coupling of an aldehyde, an amine, and an alkyne as well as in Conia-ene reaction.

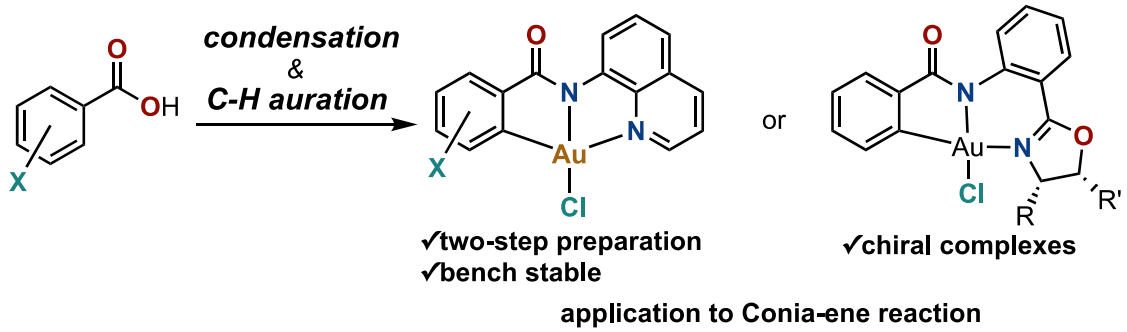

Application to Conia-ene reaction

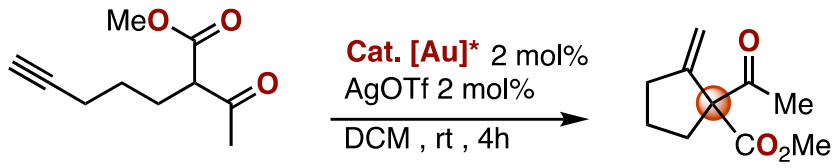

Chapter 3: Aminochlorination of Alkenes via photoirradiation

I have developed an *N*-internal vicinal aminochlorination of terminal alkenes using *N*-chloro-(fluorenone imine) as both aminating and chlorinating agents. The reaction does not require any catalyst, and only visible- light irradiation is necessary for the reaction. This simple protocol introduces an imine moiety exclusively at the internal position and affords the corresponding free primary amines after imine hydrolysis under mild conditions. Functionalization of the amino group and transformation of the alkyl chloride moiety were possible, demonstrating the potential utility of the products.

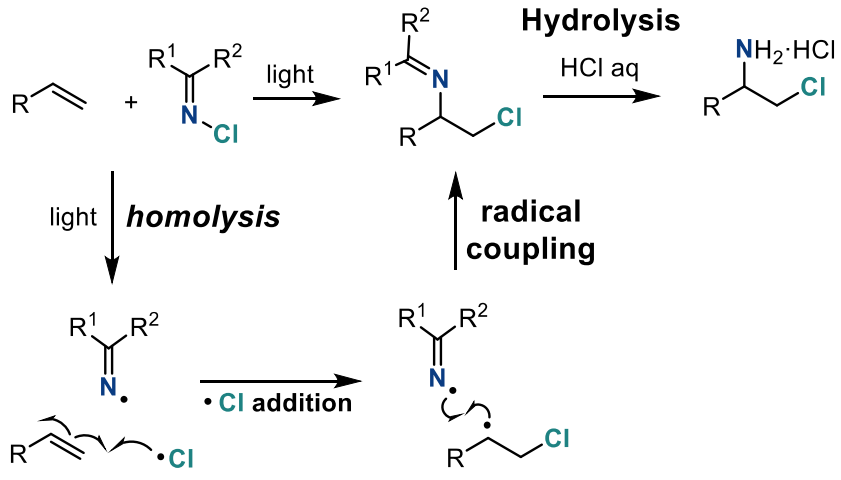

References

[1] Shimizu, Y.; Kanai, M. *Tetrahedron Lett*. **2014**, 55, 3727-3737.

[2] Phipps, R. J.; McMurray, L.; Ritter, S.; Duong, S. R.; Gaunt, M. J. *J. Am. Chem. Soc*. **2012**, *134*, 10773–10776.

[3] Suero, M. G.; Bayle, E. D.; Collins, B. S. L.; Gaunt, M. J. *J. Am. Chem. Soc.* **2013**, *135*, 5332–5335.

[4] Alexanian, E. J.; Lee, C.; Sorensen, E. J. *J. Am. Chem. Soc.* **2005**, *127*, 7690–7691.

[5] Streuff, J.; Hövelmann, C. H.; Nieger, M.; Muniz, K. *J. Am. Chem. Soc.* **2005**, *127*, 14586–14587.

[6] Yin, G.; Mu, X.; Liu, G. *Acc. Chem. Res.* **2016**, *49*, 2413–2423.

[7] Chen, C.; Luo, Y.; Fu, L.; Chen, P.; Lan, Y.; Liu, G. *J. Am. Chem. Soc.* **2018**, *140*, 1207−1210.

[8] Kennedy-Smith, J. J.; Staben, S. T.; Toste, F. D. *J. Am. Chem. Soc.* **2004**, *126*, 4526–4527.

[9] Staben, S. T.; Kennedy-Smith, J. J.; Toste, F. D. *Angew. Chem. Int. Ed.* **2004**, *43*, 5350–5352.

[10] Miles, D. H.; Veguillas, M.; Toste, F. D. *Chem. Sci*. **2013**, *4*, 3427.

[11] Lee, J. H.; Choi, S.; Hong, K. B. *Molecules.,* **2019**, *24*, 2634.

[12] Farid, U.; Wirth, T. *Angew. Chem. Int. Ed.* **2012**, *51*, 3462 –3465.

[13] Cui, J.; Jia, Q.; Feng, R.-Z.; Liu, S.-S.; He, T.; Zhang, C. *Org. Lett.***2014**, *16*, 1442–1445.

[14] Kitamura, T.; Miyake, A.; Muta, K.; Oyamada, A. J. *J. Org. Chem*. **2017**, *82*, 11721–11726.

[15] Mennie, K. M.; Banik, S. M.; Reichert, E. C.; Jacobsen, E. N. *J. Am. Chem. Soc.* **2018**, *140*, 4797–4802.

[16]Patra, T.; Das, M.; Daniliuc, C. G.; Glorius, F. *Nat Catal.* **2021**, *4*, 54–61.

[17] Li, J.; Yuan, Y.; Bao, X.; Sang, T.; Yang, J.; Huo, C. *Org. Lett.* **2021**, *23*, 3712−3717.

Chapter 2

Development of C,N,N-Cyclometalated Gold(III) for Au(III)-Catalyzed C-C Multiple Bond Functionalization

2.1 Introduction

Gold catalysts are a fascinating area of study in the field of chemistry due to their unique properties. In particular, they display strong π acidity **[1]**, making them especially useful for certain reactions. However, two distinct types of gold catalysts exist: Au(I) and Au(III).

Au(I) catalysts have been extensively researched, and a variety of complex structures have been developed using different types of ligands. Notably, phosphines and N-heterocyclic carbenes (NHCs) have been used to form these Au(I) complexes.**[2]** NHCs, for instance, are particularly interesting because of their strong σ-donor and weak π-acceptor properties, making them ideal ligands for Au(I) catalysts.

While gold(I) catalysis has established itself as a robust tool in synthetic chemistry, gold(III) catalysis remains less explored, primarily due to its high electrophilicity,**[3]** which leads to instability of the complex and can result in undesirable reductive elimination affording gold(I). For synthesis of stable Au(III) complexes, the use of structurally rigid pincer ligands is an effective approach, leading to suppression of reductive elimination. The synthesis of stable cyclometalated gold(III) complexes is feasible, particularly when using structurally rigid pincer ligands. These types of ligands can suppress reductive elimination **[4]**, enhancing the stability of the Au(III) complex.

Conventionally, the synthesis of these stable Au(III) complexes involves a two-step process that begins with the formation of a mercury complex, which is then transmetalated to gold. This method, however, is less than ideal due to the toxicity and hazardous handling associated with mercury.**[5]** An alternative method involves the direct complexation between a ligand and an Au(III) salt via a process known as C-H auration (Figure 2.1). This reaction allows for the direct insertion of gold into the carbon-hydrogen bond of an organic molecule. Not only does this method bypass the need for mercury, making it a safer alternative, but it's also a more convenient and efficient approach to creating stable Au(III) complexes. Moreover, this strategy is in line with the principles of green chemistry, reducing the use of toxic materials. **[6]**

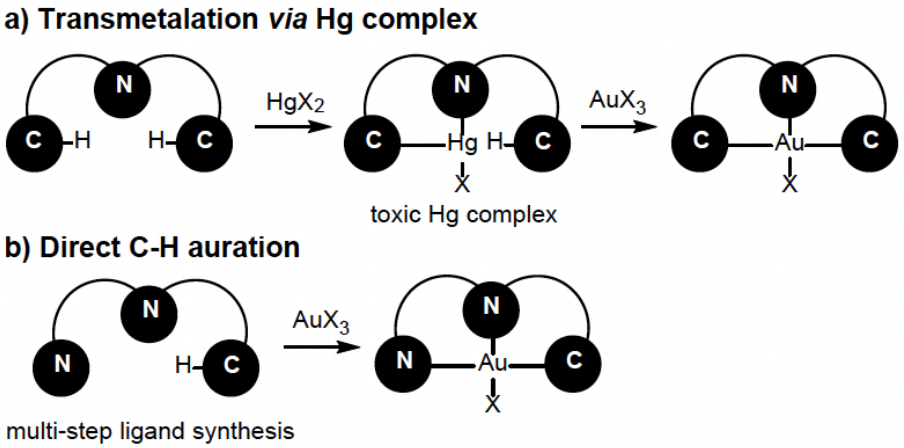

Figure 2.1: synthesis of Au(III) pincer complexes .

However, derivatization of Au(III) pincer complexes, synthesized by the direct C-H auration method, can be challenging due to the complex and multi-step process involved in ligand synthesis. For effective catalytic reaction development, it's crucial to thoroughly understand the steric and electronic effects of the catalysts. However, a readily derivatizable Au(III) pincer complex has been hard to come by due to these challenges.

The author offers a solution to this issue by developing the synthesis of novel neutral C,N,N Au(III) complexes. This is accomplished through direct C-H auration, using *N*-(8-quinolinyl)benzamide derivatives as ligands. This strategy significantly simplifies the synthesis process.**[7]** *N*-(8-quinolinyl)benzamide derivatives can be synthesized by condensing the corresponding carboxylic acids and 8-aminoquinoline. This means that the Au(III) complexes can be obtained in just two steps from commercially available carboxylic acids, streamlining the process considerably.

Furthermore, the author explores the synthesis of chiral Au(III) complexes using chiral *N*-(2-(oxazolin-2-yl)phenyl)benzamide derivatives as ligands. The creation of chiral complexes broadens the potential applications of these catalysts, as chirality plays a crucial role in many biological systems and pharmaceuticals.

The catalytic activity of these novel Au(III) complexes was demonstrated in two key reactions: a three-component coupling of an aldehyde, an amine, and an alkyne (also known as the A^3 reaction) **[8]**, and in a C-C multiple bond functionalization via the Conia-ene reaction.

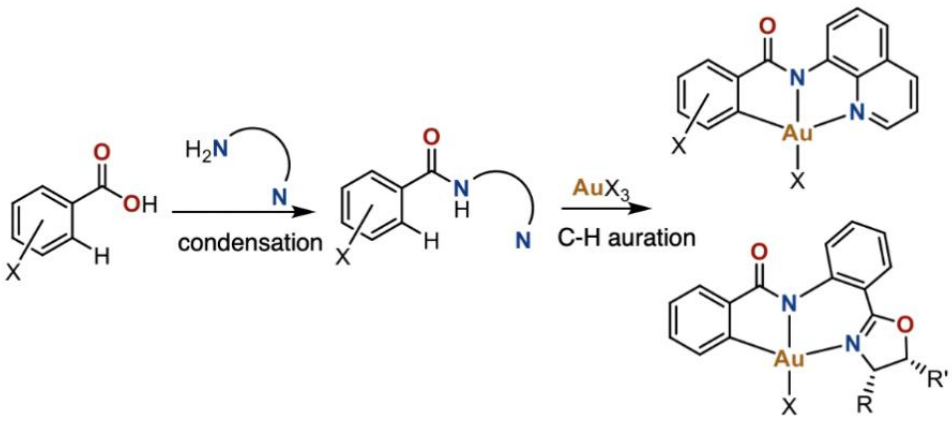

Figure 2.2: Direct C-H auration using N-(8-quinolinyl)benzamide derivatives as ligands for Au(III) pincer complexes .

2.2 Results and Discussion

2.2.1 Complex formation

Complexation reactions were examined using *N*-(8-quinolinyl)benzamide **1a** and $NaAuCl_4 \cdot 2H_2O$ in various solvents at 160 °C. The C,N,N Au(III) complex **2a** was synthesized in toluene, although with an inseparable byproduct (<43% yield). In DMF, no production of **2a** was observed, while a trace amount was obtained in MeCN, but without any byproduct. The addition of water to acetonitrile enhanced the solubility of $NaAuCl_4 \cdot 2H_2O$ and significantly increased reactivity, leading to a 63% yield of **2a**. However, the reaction also resulted in the formation of metallic gold in the mixture. Reducing the reaction temperature to 80 °C successfully eliminated the formation of metallic gold, yielding **2a** at 53%. Considering possible protodeauration of **2a** due to in situ generated HCl, the authors investigated adding a base. While potassium carbonate inhibited the reaction completely, the addition of a bulky weak base, potassium pivalate, improved the yield to 65%. Notably, compound **2a** was found to be stable and could be stored under air for at least two years.

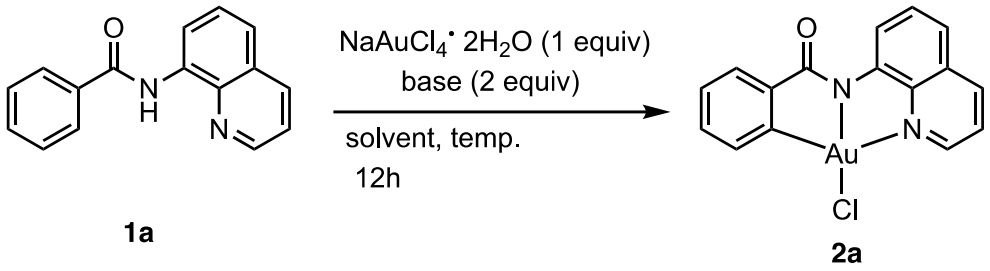

1a **2a**

entry	solvent	temp. (°C)	base	yield (%)
1	Toluene	160	none	43
2	DMF	160	none	0
3	CH_3CN	160	none	trace
4	CH_3CN/H_2O 1:1	160	none	63
5	CH_3CN/H_2O 1:1	80	none	53
6	CH_3CN/H_2O 1:1	80	K_2CO_3	0
7	CH_3CN/H_2O 1:1	80	tBuCO$_2$K	65

Scheme 2.1: Optimization of Au(III) pincer complex formation. [a] **1a** (0.03 mmol), $NaAuCl_4 \cdot 2H_2O$ (0.03 mmol), solvent (0.025 M), 12 h. Yield of isolated product.

Under the optimized reaction conditions, a series of Au(III) complexes were synthesized. When electron-donating groups like tert-butyl and methoxy were introduced at the para position of benzamide, the resultant Au(III) complexes **2b** and **2c** were obtained with 81% and 65% yield respectively. However, when an electron-withdrawing chloro substituent was introduced, it inhibited the C-H auration process, leading to a significantly reduced yield of **2d** (11%). The presence of an ortho-methoxy substituent did not impact the reactivity, yielding **2e** at 61%. When a methoxy group was introduced at the meta position, two isomers, **2f** and **2f'**, were obtained in 67% yield in a 4.7:1 ratio. A 3,4,5-Trimethoxy substitution was well-tolerated, providing **2g** with a yield of 69%. Au(III) complex **2h**, a π-extended naphthyl derivative, was produced in 64% yield as a single isomer. Furthermore, a complex containing a thiophene group was also synthesized with good yield (**2i**, 70%) under the same conditions.

The C-H auration protocol was applied to synthesize chiral Au(III) complexes bearing a phenyloxazoline moiety instead of a quinoline moiety. This led to the synthesis of Au(III) complexes with isopropyl (**2j**) and benzyl (**2k**) groups on the oxazoline rings, under the same

reaction conditions, albeit with moderate yields. However, the introduction of a rigid and sterically demanding indanyl group on the ligand decreased reactivity, yielding only 14% of **2l**.

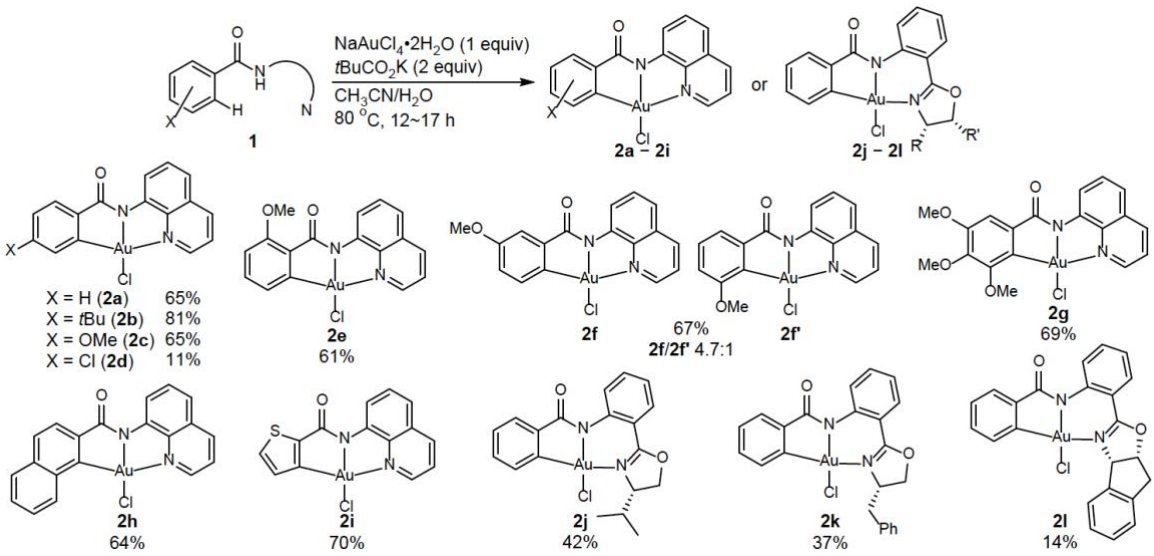

Scheme 2.2: Scope of Au(III) complexes. **1** (0.1 mmol), $NaAuCl_4 \cdot 2H_2O$ (0.1 mmol), CH_3CN/H_2O (1:1, 0.025 M), 12~17 h. Yield of the isolated product.

2.2.2 X-ray diffraction (XRD) analysis

Single crystals of **2a** and **2j** were successfully grown from $CHCl_3$ and CH_2Cl_2/Et_2O solutions, respectively. The structures of these complexes were then definitively determined using single-crystal X-ray crystallography.

The selected bond lengths and angles for complexes **2a** and **2j**, as outlined in Tables 2.1 and 2.2, are notable. As anticipated, both complexes exhibited a square planar structure, with the four bond angles around the gold atom totalling 360°. The N2-Au-Cl bond angles were nearly 180° for both complexes (2a: 179°, 2j: 176°), which is in line with expectation for square planar geometries. Interestingly, there was a slight variation in the C1-Au-N1 bond angles between the two complexes. For **2a**, the angle was slightly nonlinear at 164°, while for **2j**, it was nearly linear at 173°. Both **2a** and **2j** demonstrated Au-Cl bond lengths of 2.29 Å, which is more similar to that observed for a square planar Au(III)-Cl C,N,C pincer complex with a pyridine group in the trans position (2.28

Å)**[9]** , than to a C,C,N pincer complex with a C(sp2) anion ligand in the trans position (2.37 Å) **[10]**. This highlights the impact of different ligands on the structural properties of these complexes.

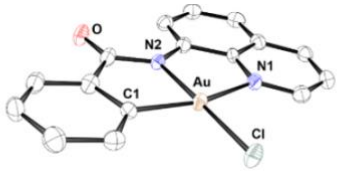

Au-Cl	2.2906(14) Å	N1-Au-N2	81.64(19) deg
Au-N1	2.114(5) Å	C1-Au-N2	82.3(2) deg
Au-N2	1.984(5) Å	C1-Au-Cl	96.97(17) deg
Au-C1	2.011(6) Å	N1-Au-Cl	99.13(14) deg
N2-Au-Cl	178.97(15) deg	C1-Au-N1	163.9(2) deg

Table 2.1 : Selected bond lengths (Å) and angles (deg) for **2a**.

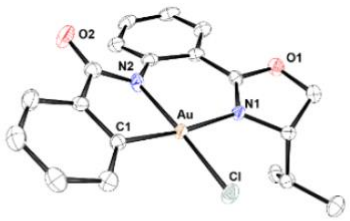

Au-Cl	2.289(2) Å	N1-Au-N2	92.4(2) deg
Au-N1	2.078(6) Å	C1-Au-N2	83.0(3) deg
Au-N2	1.997(6) Å	C1-Au-Cl	92.5(2) deg
Au-C1	2.007(7) Å	N1-Au-Cl	92.02(18) deg
N2-Au-Cl	175.53(17) deg	C1-Au-N1	173.1(3) deg

Table 2.2 : Selected bond lengths (Å) and angles (deg) for **2j**.

2.2.3 Transformations of the Au(III) complex

Next, the reactivity of the Au(III) complex **2a** was evaluated. When the hydroxy alkene **3** and **2a** were treated with 1 equivalent of $AgBF_4$, the oxyauration of the C-C double bond occurred, resulting in the formation of the alkyl Au(III) complex **4** with a yield of 48% . The reaction mechanism involves the formation of a cationic gold complex in situ, achieved by abstracting chloride anions with a silver salt, which acted as a π-acid to trigger cyclization. As anticipated, the

alkyl Au(III) complex **4** did not undergo reductive elimination and remained stable in an atmospheric environment. This observation reinforces the hypothesis about the stability of these complexes, opening doors for their potential use in various chemical reactions.

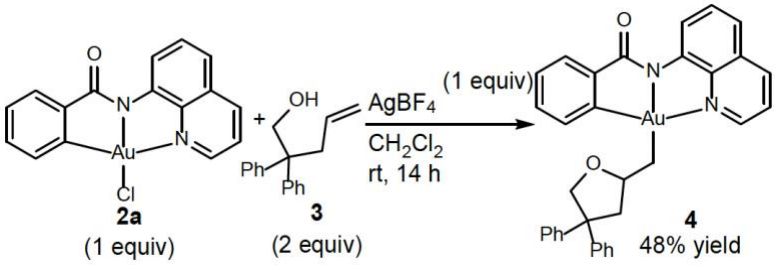

Scheme 2.3: Oxyauration of hydroxyalkene **3**.

Then an attempt to synthesize an alkynyl Au(III) complex was achieved, labeled as **6** .Initially, the desired product could not be obtained through the addition of lithium alkynide. However, a copper alkynide, generated in situ, was able to produce alkynyl Au(III) complex **6**.

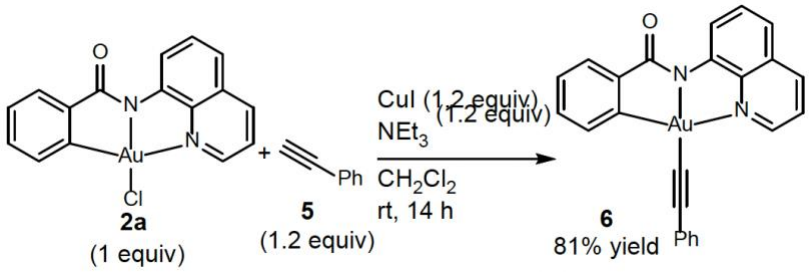

Scheme 2.4: Synthesis of alkynyl Au(III) complex.

2.2.4 Reactivity of synthesized Au(III) complexes in A^3 reaction (a three-component coupling of an aldehyde, amine, and alkyne) :

The catalytic activity of the Au(III) complex **2** was assessed in the A^3 reaction (a three-component coupling of an aldehyde, amine, and alkyne), where alkynylgold was the active nucleophile. When using 5 mol% $AuCl_3$ in the coupling of 4-bromobenzaldehyde, piperidine, and phenylacetylene in water at 40 °C, the product was obtained with a satisfactory yield of 69%. However, the use of the Au(III) complex 2a resulted in a significantly lower yield, just 27%. Other

complexes, with electron-donating substituents like tert-butyl (**2b**) and methoxy (**2c**) groups at the C5 position, provided moderate yields of 65% and 50% respectively. The presence of an electron-withdrawing 5-chloro substituent (**2d**), however, decreased the yield to 19%. A 3-methoxy substituent (**2e**) improved the yield to 74%, while a 4,5,6-trimethoxy substitution (**2g**) did not lead to yield improvement (22% yield). Interestingly, the highest catalytic activity was seen with 2h, which contains a sterically demanding naphthyl group. It gave the product with an impressive yield of 85%. The thiophene-containing complex 2i also demonstrated efficacy, with a moderate yield of 63%. When chiral Au(III) complexes was tested in the A^3 reaction, all the complexes displayed moderate catalytic activities (**2j**: 57% yield, **2k**: 39% yield, **2l**: 54% yield), with no observed enantioinduction. Lowering the catalyst loading to 0.5 mol% with the most reactive complex **2h** resulted in a reduced yield of 32% despite a prolonged reaction time of 51 hours. While the catalytic activities of these Au(III) complexes are not as high as some other reported high-performance Au(III) catalysts, the results underscore the potential for optimization of various parameters for the C,N,N Au(III) complexes, including electronic and steric factors, which could ultimately improve catalytic activity.

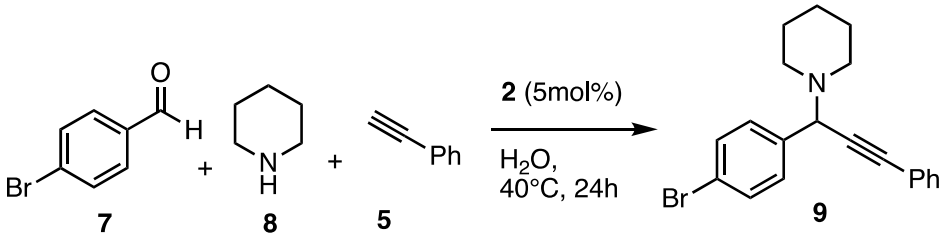

7 **8** **5** **9**

entry	complex	yield (%)
1	$AuCl_3$	69
2	**2a**	27
3	**2b**	65
4	**2c**	50
5	**2d**	19
6	**2e**	74
7	**2g**	22
8	**2h**	85 (73)
9	**2i**	63
10	**2j**	57
11	**2k**	39
12	**2l**	54 (50)
13[b]	**2h**	32

Conditions: [a] **7** (0.1 mmol), **8** (0.11 mmol), **5** (0.15 mmol), **2** (0.005 mmol), H_2O (0.5 M), 40 °C, 24 h. Yields were determined by ^1H NMR analysis using tetrachloroethane as an internal standard. Yield of the isolated product is shown in parentheses. [b] 0.5 mol% of **2h** (0.0005 mmol) was used and the reaction time was 51 h.

Scheme 2.5: Investigation of A^3 reaction using **2**.

2.2.5 Reactivity of synthesized Au(III) complexes in Conia-ene reaction :

The catalytic activities of the chiral Au(III) complexes in combination with AgOTf were investigated in the asymmetric Conia-ene reaction of **1a** as a multiple bond functionalization reaction. The Conia-ene products were obtained with yields of **2b** ranging from 8% to 46% depending on the catalysts. However, almost no induction of enantioselectivity was observed (6% ee at most when Au(III) complex bearing indanyl moietywas used. The lack of enantioselectivity could be attributed to the

almost planar geometry of the complex, as demonstrated by shown in the side view of the XRD (Table 2.3).

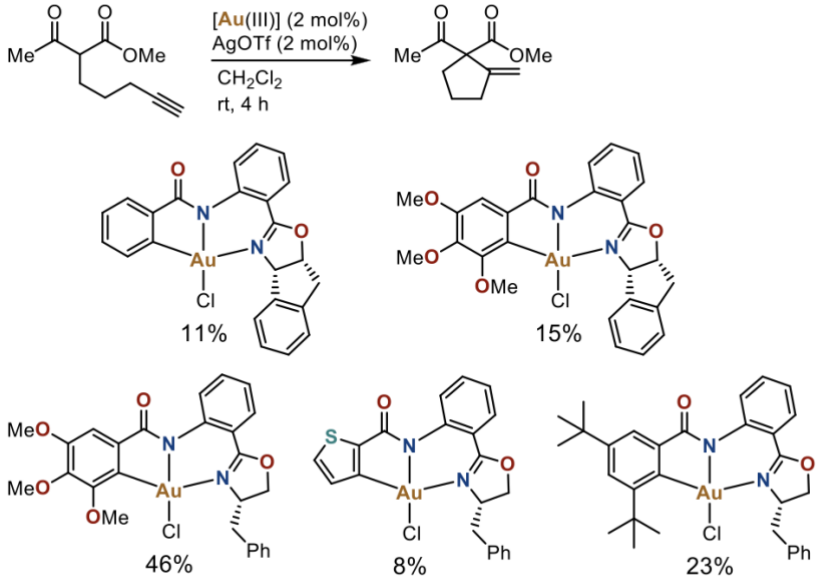

Scheme 2.6: Investigation of Conia-ene reaction using chiral Au(III) complexes .

2.3 Conclusions

In conclusion, the author successfully developed novel pincer-type C,N,N neutral Au(III) complexes. By employing a convenient ligand synthesis method, which involved the condensation of carboxylic acids with 8-aminoquinoline. This process yielded a series of Au(III) complexes with various steric and electronic properties, demonstrating the flexibility and versatility of this approach.

Furthermore, chiral Au(III) complexes were also synthesized using *N*-(2-(oxazolin-2-yl)phenyl)benzamide derivatives. The authors demonstrated the π-acidity of the cationic Au(III) complex generated in situ by performing the oxyauration of hydroxy alkene 3 in the presence of $AgBF_4$.

The author also conducted an investigation into a catalytic A^3 reaction using the Au(III) complex **2**, which clearly indicated that substituents on the benzamide moiety could impact the catalytic activity of the complex and also tested its reactivity in C-C multiple bonds functionalization through Conia-ene reaction .

2.4 Experimental Section

2.4.1 Instrumentation and Chemicals

NMR spectra were recorded on a JEOL ECX-400, operating at 400 MHz for ^1H NMR and 100.5 MHz for ^{13}C NMR. Chemical shift values for ^1H and ^{13}C are referenced to Me4Si. Chemical shifts are reported in δppm. Mass spectra were obtained with JEOL JMS-T100GCV at GC-MS & NMR Lab., Research Faculty of Agriculture, Hokkaido University and Thermo Fisher Scientific Exactive, JEOL JMS-T100GCV at the Instrumental Analysis Division, Global Facility Center, Creative Research Institution, Hokkaido University. TLC analyses were performed on commercial glass plates bearing 0.25-mm layer of Merck Silica gel $60F_{254}$. Silica gel (Kanto Chemical Co., Silica gel 60 N, spherical, neutral) was used for column chromatography.

All reactions were carried out under nitrogen or argon atmosphere. Materials were obtained from commercial suppliers or prepared according to standard procedures unless otherwise noted.

2.4.2 General Procedure for the Synthesis of Au(III) Complex 2

To a sealed tube, 1a (24.8 mg, 0.1 mmol), $NaAuCl_4 \cdot 2H_2O$ (39.8 mg, 0.1 mmol), potassium pivalate (19.6 mg, 0.2 mmol), CH_3CN (2 mL), and H_2O (2 mL) were added. The mixture was stirred for 17 h at 80 °C and then cooled to room temperature. The precipitate was filtered, washed with methanol, and dried in vacuo to give 2a as a yellowish brown solid (31.1 mg, 65% yield).

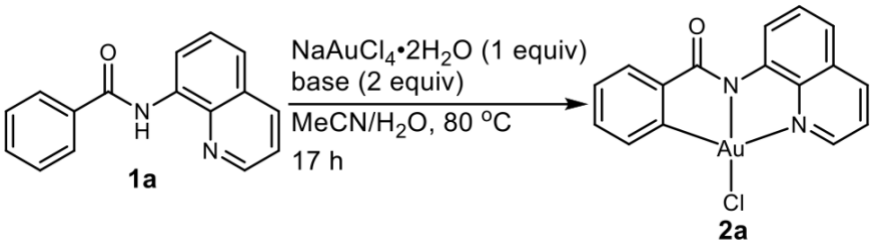

Characterization of Au(III) Complex 2

Due to the low solubility of the complexes to any solvent, ^{13}C NMR data are not clear enough even after >30,000 scans with saturated concentration for several compounds. For such compounds, all visible peaks of ^{13}C NMR are listed.

Based on COSY, HMQC, and HMBC, every peak is assigned as follows for 2c.

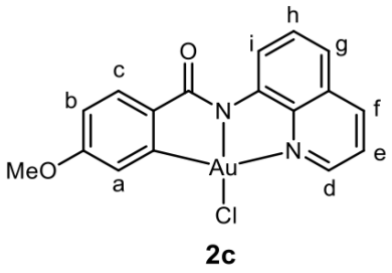

33.2 mg, 65% yield. (17 h)

^{1}H NMR ($CDCl_3$, 400 MHz): δ 9.13 (dd, *J* = 1.8, 4.6 Hz, 1H, *Ar*$_d$), 9.01 (d, *J* = 7.6 Hz, 1H, *Ar*$_i$), 8.48 (d, *J* = 1.4, 8.2 Hz, 1H, *Ar*$_f$), 7.70 (dd, *J* = 5.0, 8.2 Hz, 1H, *Ar*$_e$), 7.67 (dd, *J* = 8.2, 8.2 Hz, 1H, *Ar*$_h$), 7.52 (d, *J* = 8.0 Hz, 1 H, *Ar*$_c$), 7.48 (d, *J* = 8.0 Hz, 1 H, *Ar*$_g$), 7.40 (d, *J* = 2.4 Hz, 1 H, *Ar*$_a$), 6.87 (dd, *J* = 2.4, 8.4 Hz, 1H, *Ar*$_b$), 3.90 (s, 3H, O*Me*).

^{13}C NMR (100.5 MHz, $CDCl_3$) δ 174.24 (*C*=O), 161.48 (C_{quat}–OMe), 146.50 (Ar_d), 144.74 (C_{quat}), 144.24 (C_{quat}), 141.19 (Ar_f), 139.88 (C_{quat}–Au), 134.11 (C_{quat}–C=O), 131.45 (Ar_c), 131.02 (C_{quat}), 130.67 (Ar_h), 121.83 (Ar_e), 121.12 (Ar_i), 120.53 (Ar_g), 115.35 (Ar_a), 114.69 (Ar_b), 55.75 (O*Me*).
IR (ATR): 3063, 2937, 2835, 1653, 1578, 1504, 1463, 1326 cm^{-1}.
HRMS (FD) (m/z): Calcd for $C_{17}H_{12}AuClN_2O_2$ $[M]^+$, 508.0253 Found 508.0270.

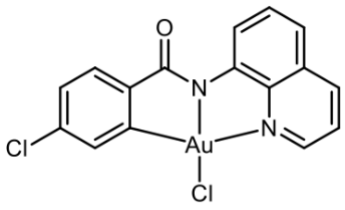

2d

Purified by flash chromatography on silica gel using gradient elution (starting with hexane to hexane/EtOAC 9/1). 5.7 mg, 11% yield. (14.5 hr)
^{1}H NMR ($CDCl_3$, 400 MHz): δ 9.15 (dd, *J* = 1.6, 4.8 Hz, 1 H), 9.01 (dd, *J* = 1.2, 8.0 Hz, 1 H), 8.50 (dd, *J* = 1.6, 8.4 Hz, 1 H), 7.85 (d, *J* = 2.4 Hz, 2H), 7.66-7.75 (m, 2H), 7.48-7.53 (m, 2H), 7.33 (dd, *J* = 2.0, 8.4 Hz, 1 H).
^{13}C NMR (100.5 MHz, $CDCl_3$) δ 151.60, 146.77, 141.45, 137.19, 131.15, 130.77, 130.40, 129.06, 121.98, 121.60, 121.18.
IR (ATR): 3066, 1654, 1573, 1503, 1463, 1382 cm^{-1}.
HRMS (ESI) (m/z): Calcd for $C_{16}H_{10}AuCl_2N_2O$ $[M+H]^+$, 512.9830 Found 512.9847.

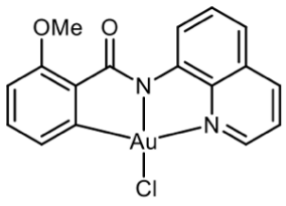

2e

31.3 mg, 61% yield. (12 h)

^{1}H NMR ($CDCl_3$, 400 MHz): δ 9.15 (dd, *J* = 1.2, 5.2 Hz, 1H), 9.10 (d, *J* = 8.0 Hz, 1H), 8.49 (d, *J* = 8.4 Hz, 1H), 7.64-7.73 (m, 2H), 7.54 (d, *J* = 8.0 Hz, 1H), 7.49 (d, *J* = 7.6 Hz, 1H), 7.28 (dd, *J* = 8.0, 8.0 Hz, 1H), 6.93 (d, *J* = 8.8 Hz, 1H), 4.00 (s, 3H).

^{13}C NMR (100.5 MHz, $CDCl_3$) δ 173.66, 159.11, 146.44, 144.60, 144.23, 141.20, 138.80, 132.15, 130.83, 130.67, 126.55, 123.32, 121.75, 121.39, 120.62, 112.38, 56.09.

IR (ATR): 3067, 2938, 2836, 1654, 1580, 1506, 1466, 1382 cm^{-1}.

HRMS (FD) (m/z): Calcd for $C_{17}H_{12}AuClN_2O_2$ $[M]^+$, 508.0253 Found 508.0245.

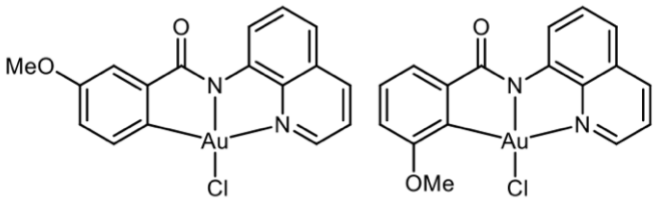

2f **2f/2f'** 4.7:1 **2f'**

33.9 mg, 67% yield. (12 h)

^{1}H NMR ($CDCl_3$, 400 MHz, major isomer): 9.13 (d, *J* = 5.2 Hz, 1H), 9.01 (d, *J* = 8.0 Hz, 1H), 8.50 (d, *J* = 8.0 Hz, 1H), 7.66-7.40 (m, 3H), 7.53 (d, *J* = 8.4 Hz, 1H), 7.13 (d, *J* = 2.0 Hz, 1H), 6.87 (dd, *J* = 2.4, 8.0 Hz, 1H), 3.88 (s, 3H).

IR (ATR): 3062, 2995, 2947, 2827, 1650, 1588, 1504, 1461, 1414, 1380 cm^{-1}.

HRMS (FD) (m/z): Calcd for $C_{17}H_{12}AuClN_2O_2$ $[M]^+$, 508.0253 Found 508.0265.

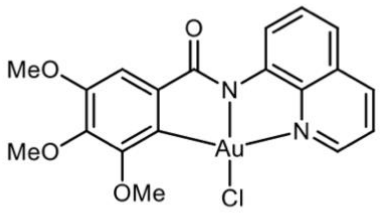

2g

39.2 mg, 69% yield. (14.5 h)

^{1}H NMR ($CDCl_3$, 400 MHz): δ 9.33 (dd, *J* = 1.2, 5.2 Hz, 1H), 8.99 (d, *J* = 7.6 Hz, 1H), 8.49 (dd, *J* = 1.2, 8.0 Hz, 1H), 7.74 (dd, *J* = 4.8, 8.0 Hz, 1H), 7.67 (dd, *J* = 8.0, 8.0 Hz, 1H), 7.52 (d, *J* = 8.0 Hz, 1H), 7.10 (s, 1H), 3.97 (s, 3H), 3.95 (s, 3H), 3.92 (s, 3H).

^{13}C NMR (100.5 MHz, $CDCl_3$) δ 174.40, 154.04, 153.42, 146.31, 145.08, 144.98, 143.85, 141.26, 137.82, 130.56, 124.00, 121.73, 121.40, 121.07, 109.68, 61.87, 61.09, 56.29.

IR (ATR): 3077, 3006, 2946, 2836, 1647, 1578, 1506, 1463, 1400, 1381 cm^{-1}.

HRMS (FD) (m/z): Calcd for $C_{19}H_{16}AuClN_2O_4$ $[M]^+$, 568.0464 Found 568.0456.

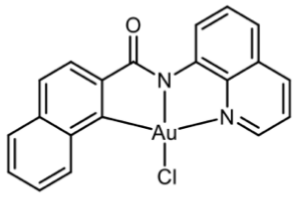

2h

34.1 mg, 64% yield. (12 h)

^{1}H NMR ($CDCl_3$, 400 MHz): δ 9.42 (d, *J* = 8.4 Hz, 1H), 9.39 (dd, *J* = 1.2, 4.8 Hz, 1H), 9.06 (d, *J* = 7.6 Hz, 1H), 8.48 (dd, *J* = 1.6, 8.4 Hz, 1H), 7.77-7.83 (m, 2H), 7.75 (dd, *J* = 4.8, 8.0 Hz, 1H), 7.63-7.71 (m, 2H), 7.50-7.62 (m, 3H).

^{13}C NMR (100.5 MHz, $CDCl_3$) δ 175.62, 144.94, 143.69, 141.31, 140.53, 137.18, 135.45, 134.11, 132.96, 130.96, 130.73, 130.56, 129.65, 128.33, 127.74, 126.75, 126.24, 121.72, 121.59, 121.14.

IR (ATR): 3057, 1645, 1587, 1575, 1462, 1379 cm^{-1}.

HRMS (FD) (m/z): Calcd for $C_{20}H_{12}AuClN_2O$ $[M]^+$, 528.0304 Found 528.0300.

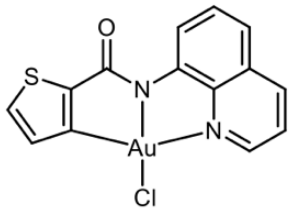

2i

34.0 mg, 70% yield. (15 h)

^{1}H NMR ($CDCl_3$, 400 MHz): δ 9.04 (d, *J* = 3.2 Hz, 1H), 8.86 (d, *J* = 7.6 Hz, 1H), 8.49 (d, *J*= 8.0 Hz, 1H), 7.64-7.74 (m, 2H), 7.61 (d, *J* = 4.4 Hz, 1H), 7.49 (d, *J* = 8.0 Hz, 1H), 7.41 (d, *J* = 4.0 Hz, 1H).

^{13}C NMR (100.5 MHz, $CDCl_3$) δ 169.37, 145.91, 144.87, 141.31, 131.24, 130.87, 127.97, 127.30, 121.86, 120.32, 120.16.

IR (ATR): 1650, 1501, 1464, 1396, 1380 cm^{-1}.

HRMS (FD) (m/z): Calcd for $C_{14}H_8AuClN_2OS$ $[M]^+$, 483.9711 Found 483.9699.

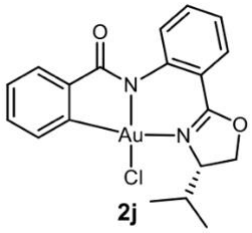

2j

22.5 mg, 42% yield. (14 h)

^{1}H NMR ($CDCl_3$, 400 MHz): δ 8.56 (dd, *J* = 9.2, 2.4 Hz, 1H), 7.84-7.91 (m, 2H), 7.58-7.63 (m, 1H), 7.49-7.56 (m, 1H), 7.27-7.35 (m, 2H), 6.99-7.06 (m, 1H), 4.96 (ddd, *J* = 3.6, 3.6, 9.2 Hz, 1H), 4.62-4.67 (m, 1H), 4.53 (dd, *J* = 9.2, 9.2 Hz, 1H), 2.60 (dsep, *J* = 3.6, 6.8 Hz, 1H), 1.00 (d, *J* = 6.8 Hz, 3H), 0.80 (d, *J* = 6.8 Hz, 3H).

^{13}C NMR (100.5 MHz, $CDCl_3$) δ 178.54, 164.28, 145.13, 140.75, 137.49, 134.63, 132.14, 130.85, 130.48, 129.85, 128.42, 124.67, 122.25, 111.98, 69.39, 68.55, 30.46, 18.57, 13.75.

IR (ATR): 2963, 1662, 1619, 1485, 1272, 1239, 1106, 741 cm^{-1}.

HRMS (FD) (m/z): Calcd for $C_{14}H_8AuClN_2OS$ $[M]^+$, 483.9711 Found 483.9699.

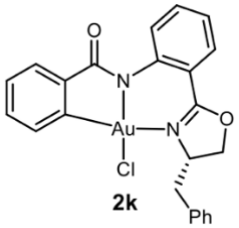

2k

21.6 mg, 13% yield. (13 h)

^{1}H NMR ($CDCl_3$, 400 MHz): δ 8.57 (dd, *J* = 8.7, 3.2 Hz, 1H), 7.91-7.95 (m, 1H), 7.83-7.89 (m, 1H), 7.60-7.64 (m, 1H), 7.51-7.57 (m, 1H), 7.30-7.35 (m, 6H), 7.23-7.29 (m, 1H), 6.99-7.05 (m, 1H), 5.18-5.24 (m, 1H), 4.61-4.66 (m, 1H), 4.45 (t, dd = 8.8 Hz, 1H), 3.58-3.65 (m, 1H), 2.67-2.75 (m, 1H).

^{13}C NMR (100.5 MHz, $CDCl_3$) δ 178.52, 164.86, 145.07, 140.63, 137.45, 135.69, 134.71, 132.21, 130.75, 130.52, 129.89, 129.45, 128.94, 128.47, 127.30, 124.92, 122.27, 112.08, 72.74, 65.26, 40.68.

IR (ATR): 1660, 1619, 1485, 1272, 1239, 1112, 740 cm^{-1}.

HRMS (FD) (m/z): Calcd for $C_{14}H_8AuClN_2OS$ $[M]^+$, 483.9711 Found 483.9699.

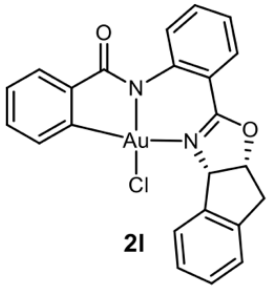

2l

8.3 mg, 14% yield. (12 h)

^{1}H NMR ($CDCl_3$, 400 MHz): δ 8.51 (dd, *J* = 1.2, 8.8 Hz, 1H), 8.13 (d, *J* = 7.2 Hz, 1H), 7.96-8.02 (m, 1H), 7.90 (dd, *J* = 1.6, 8.4 Hz, 1H), 7.59-7.64 (m, 1H), 7.49 (ddd, *J* = 1.6, 7.2, 8.8 Hz, 1H), 7.29-7.37 (m, 5H), 6.99 (ddd, *J* = 0.8, 6.8, 8.4 Hz, 1H), 6.51 (d, *J* = 6.8 Hz, 1H), 5.66-5.70 (ddd, *J* = 0.8, 5.6, 6.8 Hz, 1H), 3.62 (d, *J* = 17.6 Hz, 1H), 3.54 (dd, *J* = 5.6, 17.6 Hz, 1H).

^{13}C NMR (100.5 MHz, $CDCl_3$) δ 178.42, 164.72, 144.98, 140.64, 139.09, 138.86, 137.53, 134.64, 132.19, 130.83, 130.49, 130.12, 129.72, 128.47, 128.34, 126.63, 125.28, 124.72, 122.14, 112.17, 86.66, 72.63, 38.08.

IR (ATR): 1654, 1619, 1482, 1272, 1246, 1110, 914, 745 cm^{-1}.

HRMS (FD) (m/z): Calcd for $C_{14}H_8AuClN_2OS$ $[M]^+$, 483.9711 Found 483.9699.

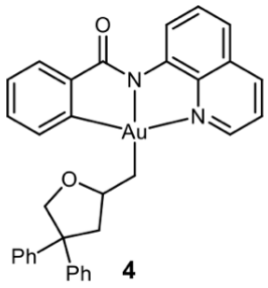

4

31.1 mg, 65% yield.

^{1}H NMR ($CDCl_3$, 400 MHz): δ 8.97 (dd, *J* = 1.2, 8.4 Hz, 1H), 8.61 (dd, *J* = 1.6, 5.2 Hz, 1H), 8.40 (dd, *J* = 1.2, 8.4 Hz, 1H), 7.71-7.75 (m, 1H), 7.65 (dd, *J* = 8.0, 8.0 Hz, 1H), 7.52 (dd, *J* = 5.2, 8.4 Hz, 1H), 7.36-7.40 (m, 2H), 7.28-7.32 (m, 2H), 7.20-7.28 (m, 9H), 7.12-7.19 (m, 1H), 4.59 (ddt, *J* = 6.4, 6.8, 8.0 Hz, 1H), 4.44 (d, *J* = 8.8 Hz, 1H), 4.39 (d, *J* = 8.8 Hz, 1H), 2.88 (dd, *J* = 6.8, 12.4 Hz, 1H), 2.59 (dd, *J* = 8.0, 12.4 Hz, 1H), 2.00 (d, *J* = 6.4 Hz, 2H).

^{13}C NMR (100.5 MHz, $CDCl_3$) δ 173.39, 146.51, 146.46, 146.08, 144.72, 140.57, 135.52, 131.33, 130.60, 129.95, 128.95, 128.41, 128.37, 127.63, 127.26, 127.07, 126.36, 126.25, 121.42, 121.14, 119.51, 80.28, 56.58, 47.57, 34.88.

IR (ATR): 2972, 1625, 1582, 1502, 1466, 1394 cm^{-1}.

HRMS (ESI) (m/z): Calcd for $C_{33}H_{28}AuN_2O_2$ $[M+H]^+$, 681.1811 Found 681.1827.

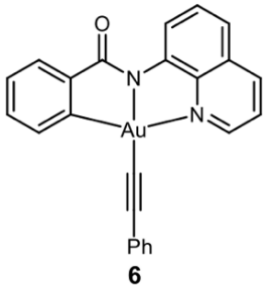

6

43.8 mg, 81% yield.

^{1}H NMR ($CDCl_3$, 400 MHz): δ 9.24 (dd, *J* = 1.2, 4.8 Hz, 1H), 9.02 (dd, *J* = 1.6, 8.4 Hz, 1H), 8.50 (dd, *J* = 1.2, 8.4 Hz, 1H), 7.94 (dd, *J* = 1.6, 8.0 Hz, 1H), 7.65-7.72 (m, 2H), 7.59-7.64 (m, 3H), 7.49 (dd, *J* = 1.2, 8.0 Hz, 1H), 7.26-7.40 (m, 5H).

^{13}C NMR (100.5 MHz, $CDCl_3$) δ 174.94, 148.32, 146.40, 145.12, 144.47, 140.95, 136.20, 133.78, 132.28, 131.84, 131.26, 130.77, 130.04, 128.30, 128.23, 127.51, 125.35, 121.92, 121.70, 120.35, 97.94, 96.44.

IR (ATR): 3053, 2989, 1640, 1594, 1582, 1501, 1487, 1462, 1450, 1441, 1384 cm^{-1}.

HRMS (ESI) (m/z): Calcd for $C_{24}H_{16}AuN_2O$ $[M+H]^+$, 545.0923 Found 545.0937.

Single Crystal XRD Analysis of 2a

A suitable crystal was mounted with liquid paraffin on a MiTeGen MicroMounts and transferred to the goniometer in a nitrogen stream at 123(2) K. Measurement was made on a RIGAKU XtaLAB Synergy-DW system with 1.2 kW PhotonJet-DW microfocus rotating anode using graphite monochromated Mo-K_a radiation (λ = 0.71073 Å) and HyPix-6000HE detector. Cell parameters were determined and refined, and raw frame data were integrated using CrysAlis^{Pro} (Agilent Technologies, 2010). The structures were solved by direct methods with SHELXT**[11]** and refined by full-matrix least-squares techniques against F^2 with SHELXL-2018/3**[12]** by using Olex2 software package.**[13]** The non-hydrogen atoms were anisotropically refined, and hydrogen atoms were placed using AFIX instructions. Crystal data and structure refinement parameters are in Table 2.3. The ORTEP-3 program was used to draw the molecule structures in Table 2.3 and Figure 2.3.**[14]**

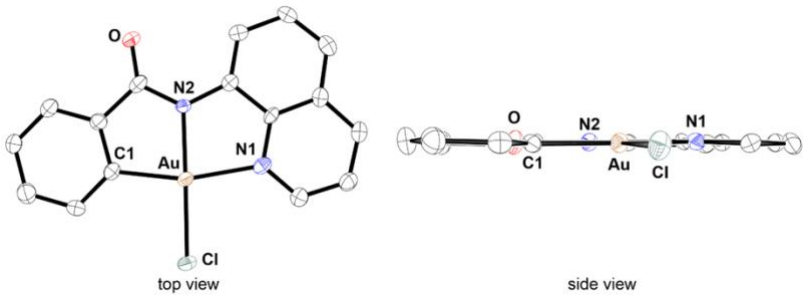

Figure 2.3 ORTEP drawing of **2a** showing 50% probability thermal ellipsoids. All hydrogen atoms were omitted for clarity. Selected bond lengths (Å) and angles (deg.) for **2a**: Au–Cl, 2.2906(14); Au–N1, 2.114(5); Au–N2, 1.984(5); Au–C1, 2.011(6); N1–Au–N2, 81.64(19); C1–Au–N2, 82.3(2); C1–Au–Cl, 96.97(17); N1–Au–Cl, 99.13(14).

Table 2.3 Crystal Data and Data Collection Parameters of **2a**

empirical formula	$AuClC_{16}H_{10}N_2O$	D_{calcd}, g/cm^{-3}	2.390
CCDC number	2107007	μ[Mo-$K\alpha$], mm^{-1}	0.71073
formula weight	478.68	T, K	123(2)
crystal system	triclinic	crystal size, mm	0.20 × 0.20 × 0.04
space group	P-1(#2)	θ range for data collection (deg.)	2.496 to 29.460
a, Å	7.5282(2)	no. of reflections measured	13259
b, Å	9.1582(2)	unique data (Rint)	3110 (0.1096)
c, Å	11.0656(3)	data/restraints/parameters	3110 / 0 / 191
α, deg.	99.367(2)	$R1$ ($I > 2.0\sigma(I)$)	0.0345
β, deg.	101.904(2)	$wR2$ ($I > 2.0\sigma(I)$)	0.0765
γ, deg.	112.400(2)	$R1$ (all data)	0.0400
V, Å^3	665.16(3)	$wR2$ (all data)	0.0788
Z	2	GOF on F^2	1.065

$R1 = (\mathrm{S}||Fo|-|Fc||)/(\mathrm{S}|Fo|)$. $wR2 = [\{\mathrm{S}w(Fo^2-Fc^2)^2\}]/(\mathrm{S}w(Fo^4)\}]^{1/2}$.

References :

[1] D. Pfl.sterer, A. S. K. Hashmi, *Chem. Soc. Rev.* **2016**, *45*, 1331–1367.

[2] (a) M. N. Hopkinson, J. E. Ross, G. T. Giuffredi, A. D. Gee, V. Gouverneur, *Org.Lett.* **2010**, 12, 4904–4907.

(b) J. Guenther, S. Mallet-Ladeira, L. Estevez, K. Miqueu, A. Amgoune, D. Bourissou, *J. Am. Chem. Soc*. **2014**, 136, 1778–1781.

(c) C.-Y. Wu, T. Horibe, C. B. Jacobsen, F. D. Toste, *Nature* **2015**, 517, 449–454.

[3] C. Michon, F. Medina, M.-A. Abadie, F. Agbossou-Niedercorn, *Organometallics* **2013**, 32, 5589–5600.

[4] Kumar, R.; Nevado, C. *Angew. Chem. Int. Ed.* **2017**, 56, 1994.

[5] (a) Wong, K.-H.; Cheung, K.-K.; Chan, M. C.-W.; Che, C.-M.*Organometallics* **1998**, 17, 3505.

(b) To, W.-P.; Zhou, D.; Tong, G. S.M.; Cheng, G.; Yang, C.; Che, C.-M. *Angew. Chem. Int. Ed.* **2017**, 56,14036.

[6] (a) Chan, C.-W.; Wong, W.-T.; Che, *C.-M. Inorg. Chem.* **1994**, 33,1266.

(b) Liu, H.-Q.; Cheung, T.-C.; Peng, S.-M. Che, C.-M. J. *Chem.Soc. Chem. Commun.* **1995**, 1787.

(c) Cinellu, M. A.; Zucca, A.;Stoccoro, S.; Minghetti, G.; Manassero, M.; Sansoni, M.; *J. Chem. Soc.Dalton Trans.* **1996**, 4217.

[7] (a) Zaitsev V. G.; Shavashob D.; Dauglies O. *J. Am. Chem. Soc.* **2005**,127, 13154.

(b) Roy P.; Bour J. R.; Kampf J. W.; Sanford M. S. *J. Am.Chem. Soc.* **2019**, 43, 17382.

(c) Rouquet G.; Chatani N. *Angew.Chem. Int. Ed.* **2013**, 52, 11726.

[8] (a) Lo V. K.-Y.; Liu Y.; Wong M.-K.; Che C.-*M. Org. Lett.* **2006**, 8,1529.

(b) Wei, C.; Li, C.-J. *J. Am. Chem. Soc.* **2003**, 125, 9584.

(c) Lo,V. K.-Y.; Kung, K. K.-Y.; Wong, M.-K.; Che, C.-M. *J. Organomet. Chem.***2009**, 694, 583.

(d) Ko, H.-M.; Kung, K. K.-Y.; Cui, J.-F.; Wong, M.-K.*Chem. Commun.* **2013**, 49, 8869.

(e) von Wachenfeldt, H.;Polukeev, A. V.; Loganathan, N.; Paulsen, F.; Röse, P.; Garreau, M.;Wendt, O. F.; Strand, D. *Dalton. Trans.* **2015**, 44, 5347.

(f) Price, G.A.; Brisdon, A. K.; Randall, S.; Lewis, E.; Whittaker, D. M.; Pritchard,R. G.; Muryn, C. A.; Flower, K. R.; Quayle, P. J. *Organomet. Chem.***2017**, 846, 251.

[9] Eppel, D.; Rudolph, M.; Rominger, F.; Hashmi, A. *S. K.ChemSusChem* **2020**, 13, 1986.

[10] Feuerstein, W.; Holzer, C.; Gui, X.; Neumeier, L.; Klopper, W.;Breher, F. *Chem. Eur. J.* **2020**, 26, 17156.

[11] Sheldrick, G. M. SHTLXT-Integrated space-group and crystal-structure determination. *Acta Cryst.* **2015**, *A71*, 3–8.

[12] Sheldrick, G. M. Crystal structure refinement with SHELXL. *Acta Cryst.* **2015**, C*71,* 3–8.

[13] Dolomanov, O. V.; Bourhis, L. J.; Gildea, R. J.; Howard, J. A. K.; Puschmann, H. OLEX2: a complete structure solution, refinement and analysis program. *J. Appl. Crystallogr.* **2009**, *42,* 339–341.

[14] ORTEP3: Farrugia, L. J. *J. Appl. Crystallogr.* **1997**, *30*, 565.

Chapter 3

Catalyst-Free Visible Light-Induced Aminochlorination of Alkenes

3.1 Introduction :

Nitrogen plays a vital role in various fields, including agrochemicals, drug molecules, and synthetic materials. The ubiquity of nitrogen in these areas highlights the significance of incorporating nitrogen atom into organic compounds. The input of nitrogen atoms into medicinal compounds bears a high impact on a compound's physiological parameters, such as hydrogen bonding interactions and polarity. As a result, the atom is prevalent in drug molecules, as the fine-tuning of physicochemical properties is a crucial factor in the development of a successful drug molecule. Thus, transformations to incorporate nitrogen are a powerful part of the synthetic chemist's toolbox.

Chloroamines, and in particular vicinal chloroamines, play a crucial role in medicinal chemistry due to the unique properties they impart to organic compounds. For instance, the vicinal chloroamine motifs have been found to exhibit potent antimicrobial activity **[1]** , making it valuable target motif in the development of new antibiotics and antiseptics.

Vicinal chloroamines represent indeed compelling targets as versatile platform compounds, capitalizing on the reactivity of the alkyl chloride moiety. The synthesis of vicinal chloroamines has seen significant advancements, particularly through the aminochlorination of readily available alkenes. This transformation has witnessed important progress in the past decade, facilitated by the development of metal catalysts, organocatalysts, photocatalysts, and also catalyst-free conditions. However, the nitrogen sources employed in these reactions have predominantly led to protected amines, which pose challenges in terms of deprotection under mild reaction conditions. Consequently, there is a pressing need for a mild and convenient method that enables aminochlorination of alkenes, affording non-protected amines or amines with readily cleavable N-protecting groups.

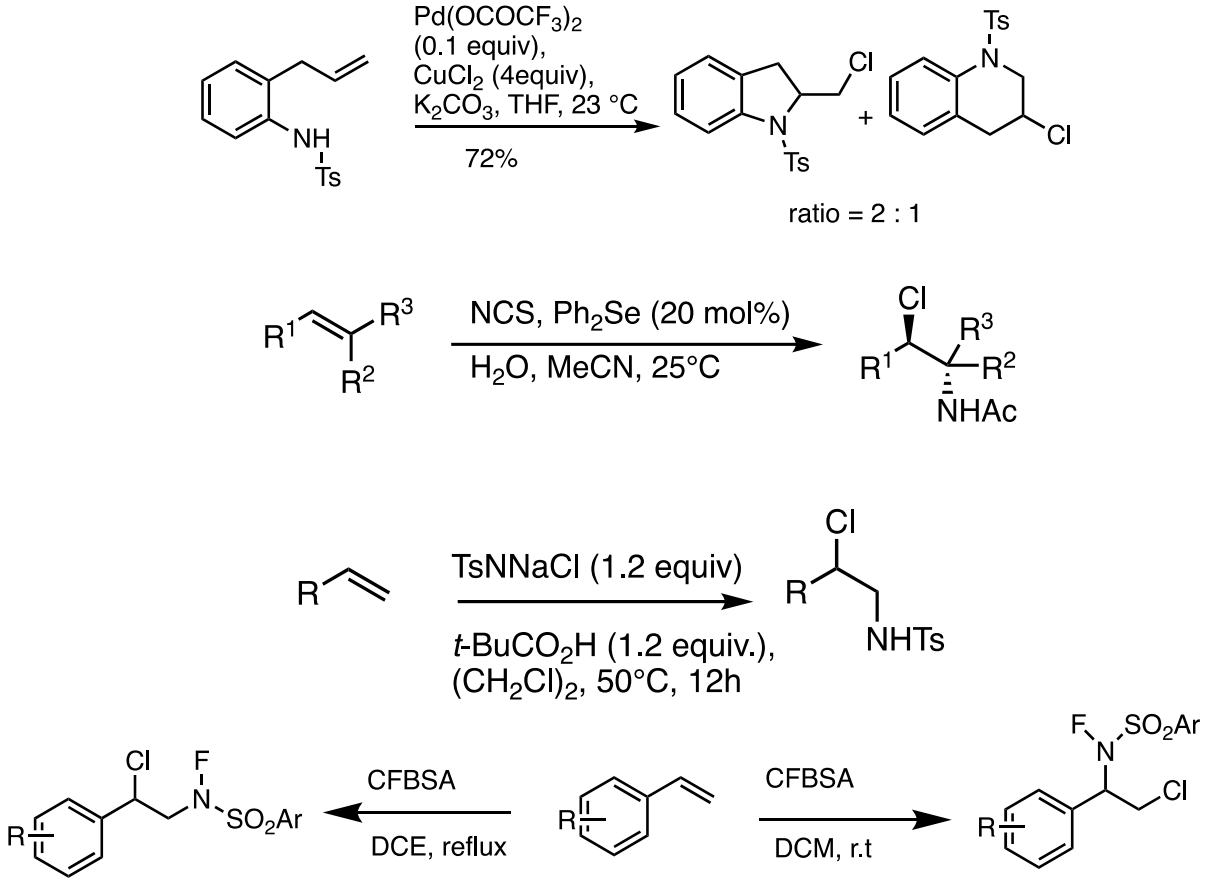

Scheme 3.1: Representative examples of aminochlorination of alkenes.

In response to the pressing need for a gentle, practical aminochlorination method producing non-protected amines or amines with easily removable *N*-protecting groups, Morandi recently disclosed an iron-catalyzed aminochlorination of alkenes that effectively produces non-protected vicinal chloroamines. **[2]** An *O*-pivaloylhydroxyamine and an alkali metal chloride were used as nitrogen and chlorine sources, respectively. These agents were used for the direct creation of unprotected secondary and tertiary 2-chloroamines from a wide array of unactivated, functionalized alkenes.

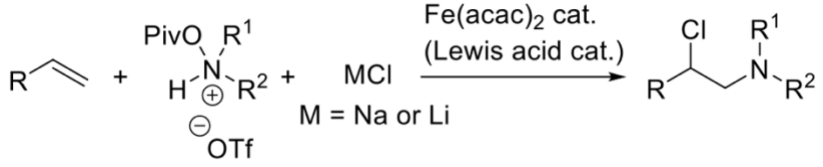

Scheme 3.2 : Iron-catalyzed *N*-terminal vicinal aminochlorination .

In the other hand, Guan, Bi, and Fu employed *N*-chloroamines as both nitrogen and chlorine sources for copper-catalyzed aminochlorinations directed by an 8-aminoquinoline amide group. **[3]**

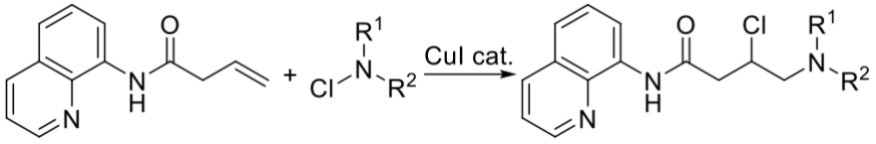

Scheme 3.3: Copper-catalyzed directed *N*-terminal vicinal aminochlorination .

Meanwhile, Leonori and co-workers discovered a photoinduced aminochlorination that directly employs various amines . An in situ formed protonated *N*-chloroamine agent served as the active entity in this reaction. **[4]**

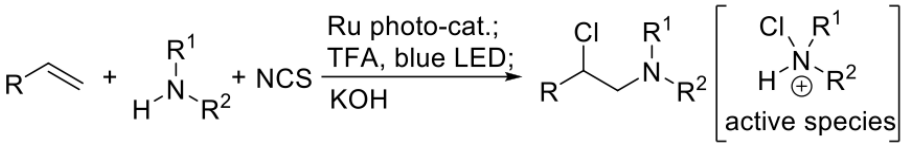

Scheme 3.4: Photocatalyst-promoted *N*-terminal vicinal aminochlorination .

All these reactions add a nitrogen atom at the terminal position. A vicinal aminochlorination that places an amino group at the internal position was accomplished only by using electrophilic N-chloroamine-based agents.

3.1.1 Catalyst-free visible light-induced Aminochlorination of Alkenes

In this context, I advanced an *N*-internal vicinal aminochlorination of terminal alkenes, employing *N*-chloro(fluorenone imine) as both aminating and chlorinating agents. The process necessitates no catalyst and relies solely on visible-light irradiation. This straightforward protocol selectively installs an imine group at the internal position, yielding corresponding free primary amines after imine hydrolysis under mild conditions. The potential utility of the products is illustrated by the feasible functionalization of the amino group and transformation of the alkyl chloride moiety.

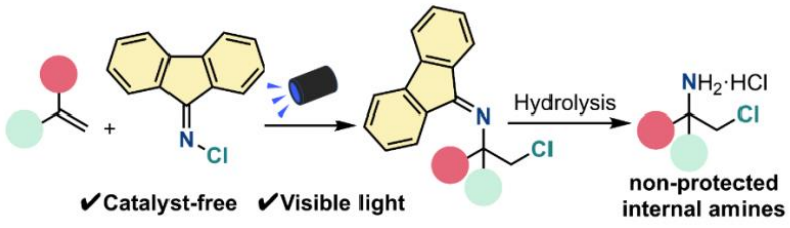

Scheme 3.5: Photoinduced *N*-internal vicinal aminochlorination of alkenes.

3.1.2 Results and Discussion

Herein, my approach involves designing an *N*-internal vicinal aminochlorination of terminal alkenes as follows. An *N*-chloroketimine, synthesized from an aromatic ketone with an extended π-system, would be photoexcited by visible light irradiation. This could lead to the homolysis of the N–Cl bond via the excited state of the *N*-chloroimine, simultaneously generating an *N*-centered iminyl radical and a Cl radical. Given that simple alkenes are reactive towards electrophilic radicals, the highly electrophilic Cl radical would likely react preferentially in the presence of the nucleophilic *N*-centered iminyl radical. The Cl radical addition would occur at the terminal position of the alkene, producing a stable internal carbon radical. This carbon radical could couple with the *N*-centered iminyl radical, yielding the internal amine product. Finally, the installed imine group would undergo hydrolysis under mild conditions to yield the corresponding primary amine.

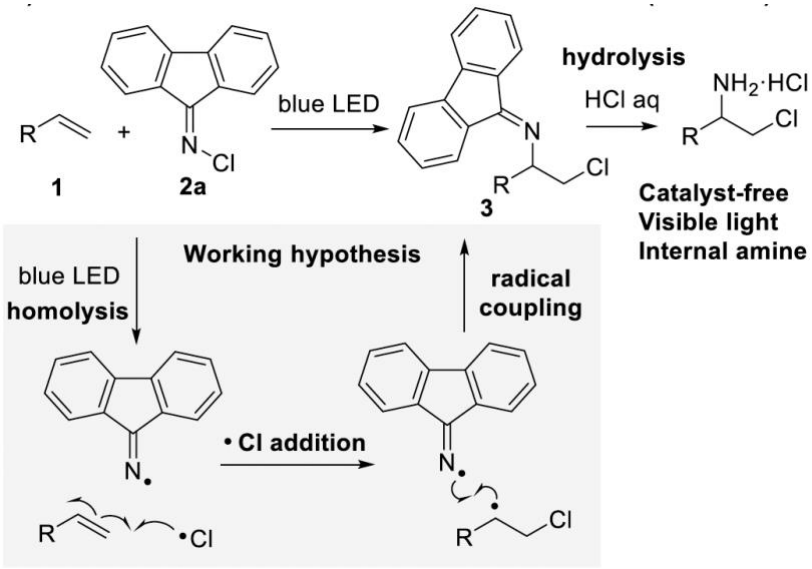

Scheme 3.6: Radical pathway for accessing *N*-internal vicinal amine.

As the synthesis of *N*-chloroketimines depends on the oxidation and chlorination of corresponding free amines as established by prior research **[5]**, structural diversity was constrained by the accessibility of the amines.

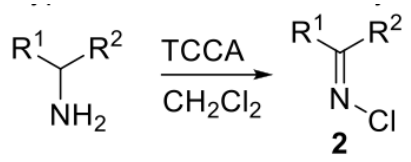

Scheme 3.7: Typical *N*-chloroketimines synthesis.

To enable a broader range of *N*-chloroketimines, I conceived the synthesis from easily available ketones via the formation of unprotected imines followed by *N*-chlorination. Bearing this in mind, a novel method for synthesizing fluorenone-derived *N*-chloroimine **2a** was developed. Consequently, $Sc(OTf)_3$-catalyzed imine formation utilizing hexamethyldisilazane (HMDS, 1.1 equiv) as a nitrogen source **[6]** was followed by *N*-chlorination with 0.4 equivalent of trichloroisocyanuric acid (TCCA), resulting in *N*-chloro(fluorenone imine) **2a** in a 93% yield in a one-pot process. Scale-up to 10 mmol was achievable without a yield decrease, albeit with a longer reaction duration for the *N*-chlorination phase. Dimethylanthracenone was similarly reactive, yielding **2b** in 63% yield. Despite xanthone being less reactive than fluorenone and dimethylanthracenone, the corresponding *N*-chloroketimine **2c** was obtained in a satisfactory yield 73% by stirring for 72 hours at 110°C with 2 equivalents of HMDS for imine formation and subsequent *N*-chlorination using 0.7 equivalent of TCCA.

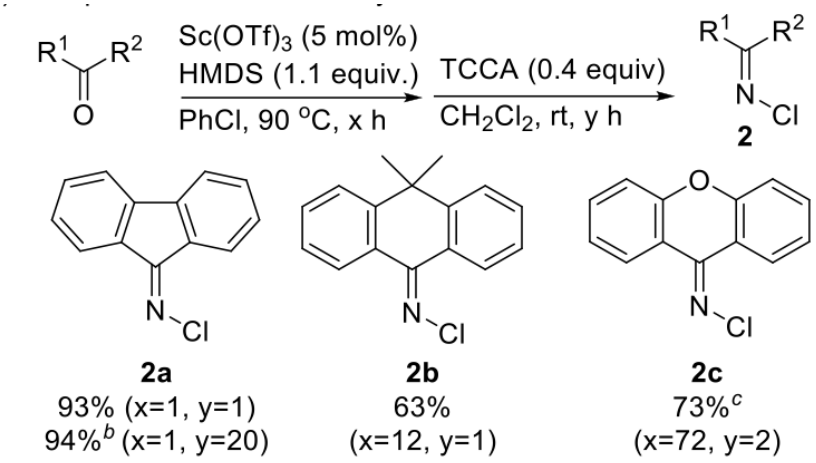

Scheme 3.8: One-Pot *N*-chloroketimine synthesis from ketones.

Subsequently, vicinal aminochlorination was examined with 1,1-diphenylethylene as the alkene substrate under blue LED irradiation. *N*-Chloro(fluorenone imine) (**2a**) resulted in the desired vicinal aminochlorination product **3a** in a 64% yield, with a vicinal dichlorination product **4a** in a 17% yield (entry 1). Conversely, anthracenone-type (**2b**) and xanthone-type (**2c**) *N*-chloroimines exhibited low reactivity, yielding **3b** and **3c**, respectively, in minimal yields (entries 2 and 3). A bicyclic derivative, *N*-chloro(tetralone imine) **2d**, also demonstrated low reactivity, yielding **3a** at only a 16% yield (entry 4). *N*-Chloroimines with flexible carbon structures, like benzophenone-type (**2e**) and acetophenone-type (**2f**) *N*-chloroimines, were completely unreactive (entries 5 and 6).

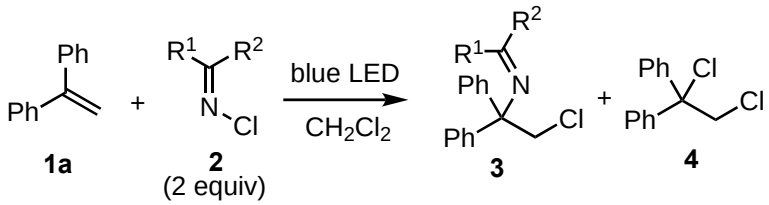

entry	2	yield (%) of 3	yield (%) of 4
1	**2a**	64	17
2	**2b**	13	9
3	**2c**	8	10
4	**2d**	16	5
5	**2e**	0	0
6	**2f**	0	0

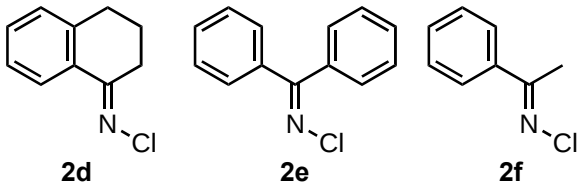

Table 3.1: Optimization of aminochlorination. [a] Conditions :**1a** (0.1 mmol), **2** (0.2 mmol), CH_2Cl_2 (0.05 M), blue LED, 12 h, **3** (aminochlorination product), **4** (dichlorination product). Yields were determined by ^1H NMR analysis using tetrachloroethane as an internal standard.

Employing **2a** as the optimal aminochlorination agent, the scope of alkenes was explored. Post photoinduced aminochlorination, raw materials were hydrolyzed to yield corresponding primary amine·HCl salts. When needed, purification was achieved using a reversed-phase (C_{18}) HPLC column under 0.1% aq. TFA/MeCN eluent conditions, resulting in products as TFA salts. The product **5a**, originating from 1,1-diphenylethylene **1a**, was isolated without HPLC purification in a 68% yield as the HCl salt. When scaled to 1 mmol, the reaction proceeded with a 47% yield. Although a 4-methyl substituent on the benzene ring was tolerated (**5b**, 57% yield), an electron-donating 4-methoxy substituent noticeably decreased the yield (**5c**, 11% yield). *p*-Chloro and fluoro substituents successfully yielded corresponding products (**5d**, 55% yield; **5e**, 72% yield). α-Methylstyrene **1f** also reacted to give **5f** in a 43% yield. Monoaryl styrene derivatives also underwent aminochlorination under the reaction conditions, albeit generally with lower yields. The reaction was tolerant of various substituents at the para position of the aryl group including electron-donating tert-butyl (**5h**, 42% yield) and methoxy (**5i**, 30% yield) groups, electron-deficient chloro (**5j**, 34% yield) and phenyl (**5k**, 29% yield) groups, and a potentially reactive chloromethyl group (**5l**, 34% yield). Conversely, an ortho-methoxy substituent (**5m**) reduced the yield to 18%. Methyl or phenyl substituents at the β-position of the styrene were compatible, delivering the products with moderate diastereoselectivities (**5n**, 39% yield, dr 6.0:1; **5o**, 35% yield,

dr 7.3:1 from trans-stilbene and 3.7:1 from cis-stilbene). A cyclic substrate, indane **1p**, provided the product **5p** with high trans-selectivity (33% yield, dr 16:1).

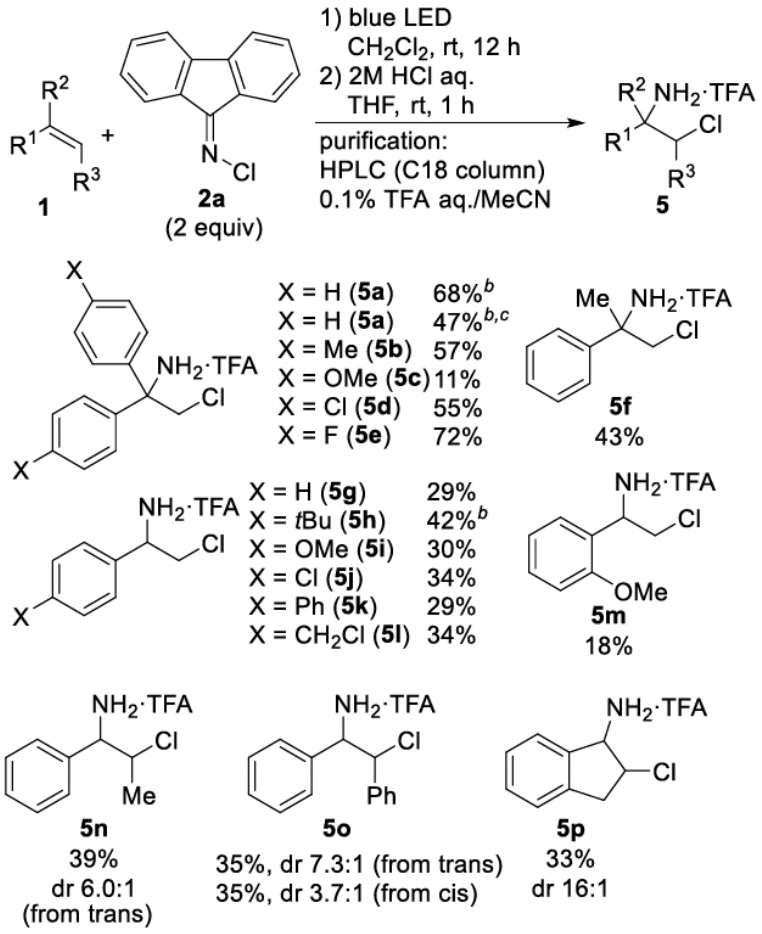

Scheme 3.9: Substrate scope .
[a] Conditions : **1** (0.3 mmol), **2** (0.6 mmol), CH_2Cl_2 (0.05 M), blue LED, 12 h. Yields of isolated products. [b] Isolated as HCl salt without HPLC purification. [c]1 mmol scale.

The vital influence of the fluorene framework of *N*-chloroimine was attributed to its photo-absorption capacity. Indeed, the UV-Vis spectrum of **2a** displayed substantial absorption in the blue LED emission range, whereas the other *N*-chloroimines exhibited considerably less or no absorption in the same region .

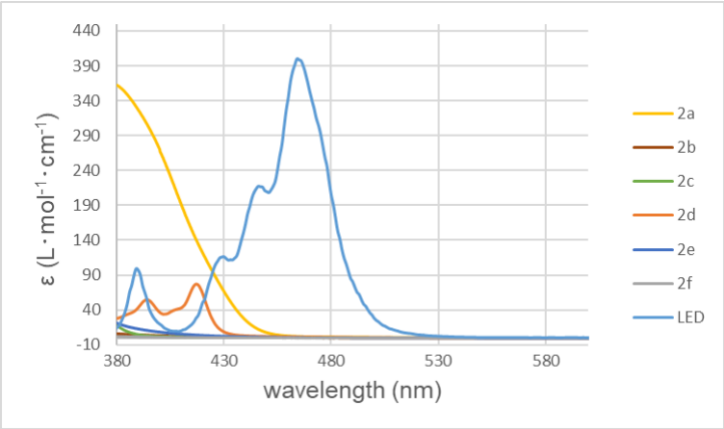

Figure 3.1: UV-Vis spectra of **2** and emission spectra of blue LED. Condition: UV-Vis spectra of **2** in CH_2Cl_2 (3 mM).

Product formation and substrate consumption were monitored by ^1H NMR spectroscopy using 1,1,2,2-tetrachloroethane as an internal standard in C_6D_6 solvent with intermittent photoirradiation (Figure 3.2). The reaction progress was only observed during the photoirradiation periods. The absence of product formation during the dark conditions confirmed the requirement of photoirradiation. However, radical chain process cannot be ruled out only by the result of light/dark experiment. **[7]**

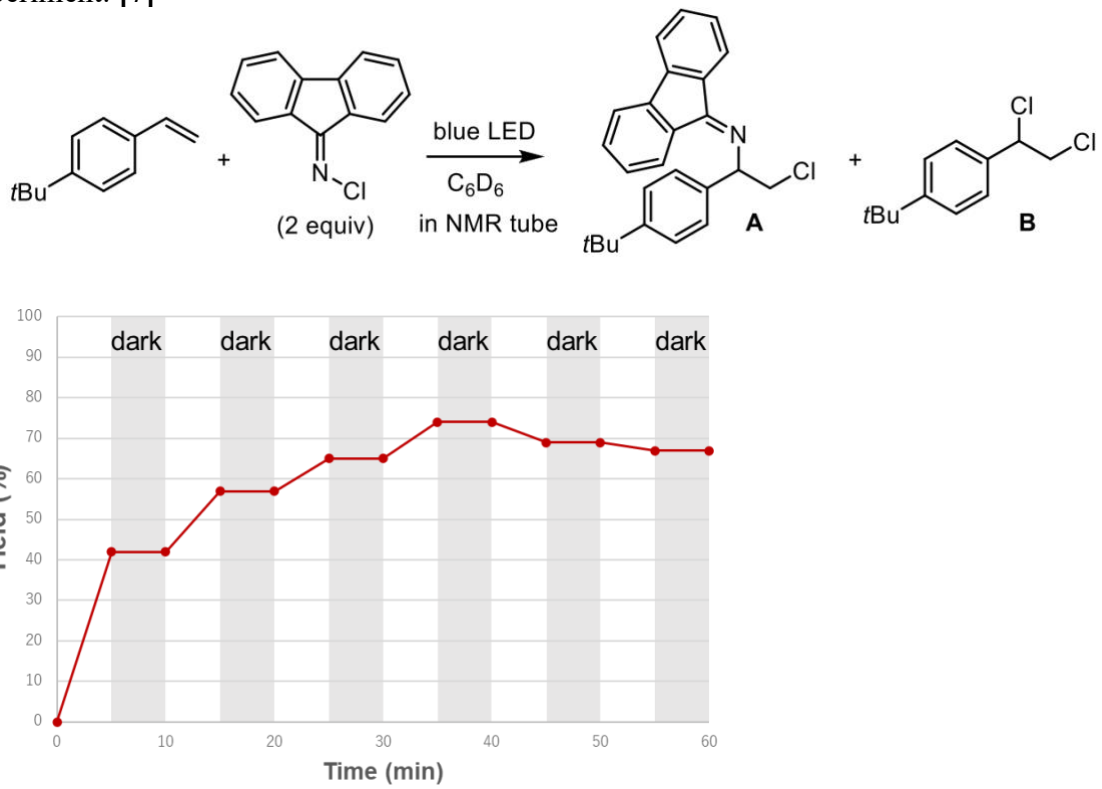

Figure 3.2 : Effect of blue LED irradiation on the reaction profile.

Transformation of aminochlorination products

Next, to assess the reactivity of the obtained aminochlorination products, using **5h** as an example. First, I added Boc and Cbz groups to the nitrogen atom, which worked well and didn't change the C–Cl bond. Then, an oxazoline (**7**) was synthesized in two steps: acylation and cyclization. The reaction yielded 59% .

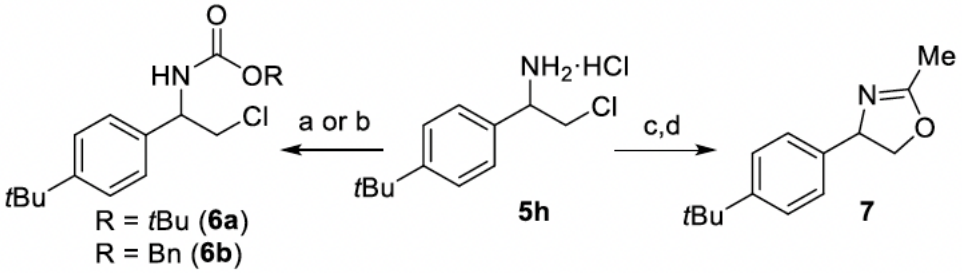

Scheme 3.10: Transformations of chloroamine **5h.** [a] Boc_2O (2 equiv), NEt_3 (2.2 equiv), CH_2Cl_2, rt, 17 h, 72% yield . [b] CbzCl (2 equiv), $NaHCO_3$ (2 equiv), THF, 0°C, 15 min, 55% yield. [c] Ac_2O (3 equiv), NEt_3 (3.5 equiv), THF, rt, 1.5 h, 74% yield . [d] NEt_3 (2 equiv), TBAI (0.5 equiv), THF, 80°C, 7 h, 80% yield.

DFT calculation

Density functional theory (DFT) calculations were performed to investigate the mechanism of Aminochlorination formation using the Gaussian 16 C.01 package at the UωB97X-D/6-31+G(d,p)/SMD(DCM) level of theory. **[8]** First, the photoinduced N–Cl scission was assessed (Figure 3.3). The N–Cl bond of the optimized structure of triplet state **2a***, which would be generated through photoexcitation and intersystem crossing, is oriented perpendicular to the π-plane of the fluorene backbone. The N–Cl homolysis from **2a*** proceeded through TS as an essentially barrierless process (0.1 kcal/mol), and an *N*-centered iminyl radical (**A**) and a chlorine radical (**B**) were generated in a slightly exergonic process (–1.5 kcal/mol relative to **2a***).

The addition of the Cl radical (**B**) to styrene (**1g**) proceeds in a barrierless manner to produce chloromethylated benzyl radical (**C**), while the addition of the iminyl radical (**A**) requires 20.4 kcal/mol to afford an aminomethylated benzyl radical (**D**) (Figure 2b). The requirement of higher energy for the iminyl radical addition than that for the Cl radical addition is consistent with our reaction design, in which the electrophilic Cl radical was expected to react preferentially in the presence of the nucleophilic *N*-centered iminyl radical. For the subsequent process, we examined two pathways that incorporate the imine moiety at the benzylic position. One is radical-radical coupling between the benzyl radical **C** and the iminyl radical **A** to produce **3g** in a highly exergonic manner. For this process, we failed to locate a transition state as expected due to the general difficulty of computations for radical-radical coupling processes. The other possibility is attack of

the radical center of **C** at the nitrogen atom of **2a**. The corresponding transition state (**TS2**) is 20.2 kcal/mol higher in Gibbs free energy relative to **C**, and subsequent elimination of the Cl radical (**B**) proceeds via a transient fluorenyl radical (**E**) to propagate a radical chain process. It should be noted that the addition of **C** to **2a** can happen at the Cl atom to produce **4g** through **TS3** (1.3 kcal/mol higher in Gibbs free energy relative to **TS2**). Since vicinal dichloride side product **4g** was obtained in meaningful amounts in the experiments, the C–Cl bond formation process at the benzylic position should be competitive with the C–N bond formation process. Although the radical chain process requires higher energy than the radical-radical coupling process, the former process cannot be excluded considering that **2a** was present in much higher concentration than iminyl radical (**A**).

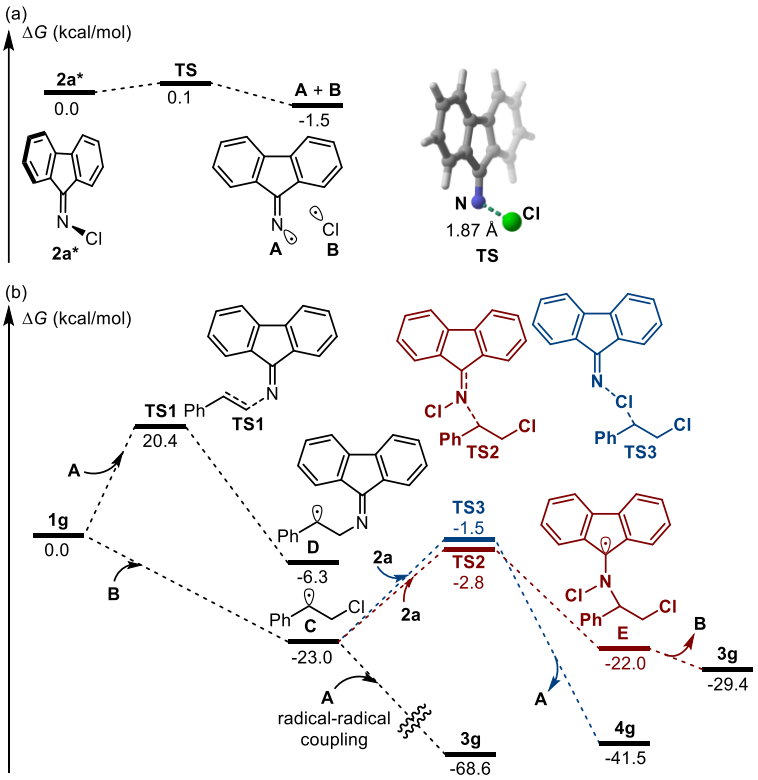

Figure 3.3: Energy diagrams for (a) radical generation and (b) radical addition to styrene.

Conclusion

In this study, I developed a method for *N*-internal vicinal aminochlorination of terminal alkenes using *N*-chloro(fluorenone imine) as both the source of amination and chlorination. This reaction is advantageous in several ways: it doesn't require any catalyst, it only needs visible-light irradiation, and it adds an imine moiety exclusively at the internal position. After this step, mild hydrolysis can remove the imine to reveal the primary amines. Moreover, it's possible to further modify the amino group and transform the alkyl chloride part, showing that the products have potential for further applications. This simple and effective method can have important implications in organic synthesis.

3.1.3 Experimental section

Instrumentation and chemicals

Nuclear magnetic resonance (NMR) spectra were recorded on a JEOL ECX-400, operating at 400 MHz for ^{1}H NMR and 100.5 MHz for ^{13}C NMR. Chemical shift values for ^{1}H and ^{13}C are referenced to Me4Si or a residual solvent peak. Chemical shifts are reported in δ ppm. Mass spectra were obtained with JEOL JMS-T100GCV or Thermo Scientific Exactive at Global Facility Center, Creative Research Institution, Hokkaido University. TLC analyses were performed on commercial glass plates bearing 0.25-mm layer of Merck Silica gel 60F_{254}. Silica gel (Kanto Chemical Co., Silica gel 60 N, spherical, neutral) was used for column chromatography. Biotage Isolera One with packed column was also used for normal phase column chromatography. HPLC purifications were conducted on a SHIMADZU HPLC system with a SHIMADZU SPD-M20A detector using YMC triart C18 column (250x10, 5 μm).

All reactions were carried out under argon atmosphere. Materials were obtained from commercial suppliers or prepared according to standard procedures unless otherwise noted.
Kessil A160WE Tuna Blue was used as the blue LED without any kind of filter for the reaction. The material of the reaction vial is borosilicate glass. The distance of the vial from light source is 4 cm.

Preparation of Substrates

General procedure for Aminochlorination Products:

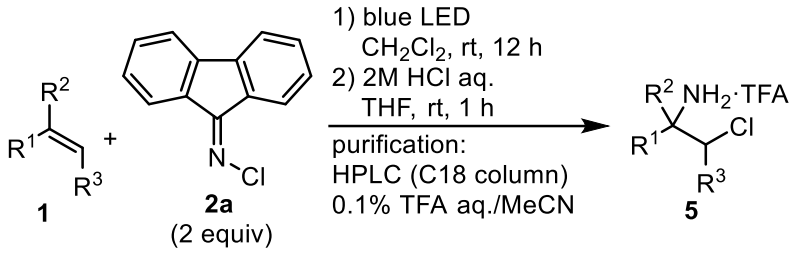

A solution of alkene **1** (0.3 mmol) and chloroimine **2a** (0.6 mmol) in CH_2Cl_2 (6 mL) was prepared in a 10 mL vial under air. The vial was flushed by argon and sealed with a Teflon-coated cap. The mixture was stirred for 12 h with blue LED (Kessil A160WE Tuna Blue) irradiation at room temperature. To the resulting brown suspension was added Et_2O, and the mixture was filtrated through a pad of celite using Et_2O eluent. The filtrate was evaporated on a rotavapor.

The obtained residue was dissolved in THF (1 mL), and 2M HCl aq. was added to the solution. After stirring for 1 h at room temperature, hexane was added to the mixture. The aqueous layer was separated and washed with hexane four times. The combined organic layer was evaporated and suspended again by hexane. The suspension was extracted with 2M HCl aq. ten times, and the combined aqueous layer was evaporated. The crude residue was purified by HPLC equipped with triart C18 column (250x10, 5 μm), 0.1% TFA aq./MeCN eluent, flow rate 4 mL/min, 5%-100%-100% 25 min-5 min, detection 200 nm.

Preparation and Characterization of Substrates

N-chloro-9*H*-fluoren-9-imine (2a)

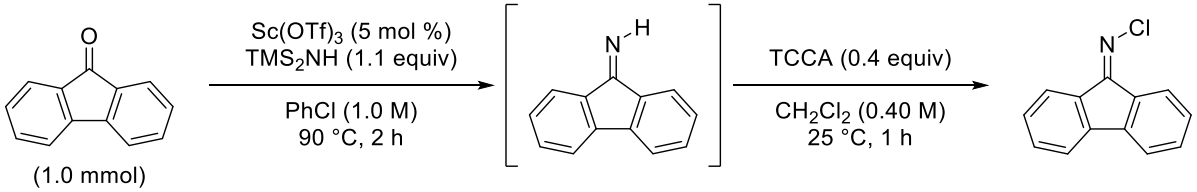

A glass test tube equipped with a magnetic stir bar was added scandium(III) trifluoromethanesulfonate ($Sc(OTf)_3$) (24.6 mg, 0.05 mmol, 0.05 equiv) and dried under vacuum using a heat gun. After cooling to room temperature, the flask was refilled with argon, and 9-

fluorenone (180 mg, 1.0 mmol, 1.0 equiv), chlorobenzene (1.0 mL), and 1,1,1,3,3,3-hexamethyldisilazane (HMDS) (0.23 mL, 1.1 mmol, 1.1 equiv) were added. The mixture was stirred at 90 °C in an oil bath for 2 h. After the consumption of 9-fluorenone was confirmed by ^{1}H NMR analysis of the crude mixture, CH_2Cl_2 (2.5 mL) was added and the mixture was stirred at 4 °C in an ice bath for 10 min. To the mixture was added trichloroisocyanuric acid (TCCA) (93.0 mg, 0.40 mmol, 0.40 equiv) at the same temperature, then the mixture was warm to 25 °C and was stirred for 1 h. The resulting mixture was diluted with water (10 mL) and extracted with CH_2Cl_2 (10 mL x 3), dried over Na_2SO_4, filtered, and concentrated under reduced pressure. The crude product was purified by silica gel flash column chromatography using hexane as an eluent to give *N*-chloro-9*H*-fluoren-9-imine **2a** as yellow solid (198 mg, 93% yield).

^{1}H NMR (500 MHz, $CDCl_3$) δ 8.75 (d, *J* = 7.5 Hz, 1H), 7.78 (d, *J* = 7.5 Hz, 1H), 7.63 (d, *J* = 7.5 Hz, 1H), 7.56 (d, *J* = 7.5 Hz, 1H), 7.51 (ddd. *J* = 7.5, 7.5, 1.0 Hz, 1H), 7.43 (ddd. *J* = 7.5, 7.5, 1.0 Hz, 1H), 7.35 (ddd, *J* = 7.5, 7.5, 1.0 Hz, 1H), 7.29 (ddd, *J* = 7.5, 7.5, 1.0 Hz, 1H).
^{13}C NMR (125 MHz, $CDCl_3$) δ 171.4, 143.8, 140.7, 136.8, 133.2, 132.3, 132.0, 129.7, 128.7, 128.4, 123.1, 120.4, 119.9.
IR (neat) 1576, 1447, 1302, 1144, 935, 781, 721, 694, 644, 631, 615, 527, 426 cm^{-1}.
HRMS (DART) *m/z*: $[M+H]^+$ Calcd for $C_{13}H_9N^{35}Cl$ 214.0418, found 214.0148, $[M+H]^+$ calcd. for $C_{13}H_9N^{37}Cl$ 216.0389, found 214.0386.

Procedure for 10 mmol Scale Synthesis

A 100 mL flask equipped with a magnetic stir bar was added scandium(III) trifluoromethanesulfonate ($Sc(OTf)_3$) (246 mg, 0.5 mmol, 0.05 equiv) and dried under vacuum using a heat gun. After cooling to room temperature, the flask was refilled with argon, and 9-fluorenone (1.80 g, 10.0 mmol, 1.0 equiv), chlorobenzene (10.0 mL), and 1,1,1,3,3,3-hexamethyldisilazane (HMDS) (2.30 mL, 11.0 mmol, 1.1 equiv) were added. The mixture was stirred at 90 °C in an oil bath for 2 h. After the consumption of 9-fluorenone was confirmed by ^{1}H NMR analysis of the crude mixture, CH_2Cl_2 (25 mL) was added and the mixture was stirred at 4 °C in an ice bath for 10 min. To the mixture was added trichloroisocyanuric acid (TCCA) (930 mg, 4.00 mmol, 0.40 equiv) at the same temperature, then the mixture was warm to 25 °C and was stirred for 20 h. The resulting mixture was diluted with water (50 mL) and extracted with CH_2Cl_2 (50 mL x 3), dried over Na_2SO_4, filtered, and concentrated under reduced pressure. The crude product was purified by silica gel flash column chromatography using hexane as an eluent to give *N*-chloro-9*H*-fluoren-9-imine **2a** as yellow solid (2.00 g, 94% yield).

***N*-chloro-10,10-dimethylanthracen-9(10*H*)-imine**

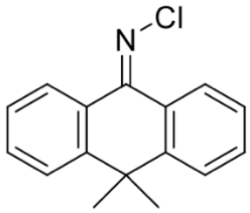

2b

162 mg, 63% yield, pale yellow oil.

^{1}H NMR (400 MHz, $CDCl_3$) δ 8.40 (dd, *J* = 1.2, 7.6 Hz, 1H) , 7.84 (dd, *J* = 1.6, 8.0 Hz, 1H), 7.67 (d, *J* = 7.6 Hz, 1H), 7.56 (d, *J* = 7.6 Hz, 1H), 7.51-7.41 (m, 2H), 7.40 (ddd, *J* = 1.2, 7.6, 7.6 Hz, 1H), 7.35 (ddd, *J* = 1.2, 7.6, 7.6 Hz ,1H) , 1,66 (s, 6H).

^{13}C NMR (100.5 MHz, $CDCl_3$) δ 169.7, 148.6, 145.6, 134.8, 130.8, 130.1, 129.9, 128.7,126.8, 125.9, 125.3, 123.9, 123.2, 39.9, 30.4.

IR (ATR) 2968, 1599, 1557, 1466, 765, 622 cm^{-1}.

HRMS (EI-TOF) *m/z*: $[M]^+$ Calcd for $C_{20}H_{16}O_3S$ 336.0820; Found 336.0834.

***N*-chloro-9*H*-xanthen-9-imine**

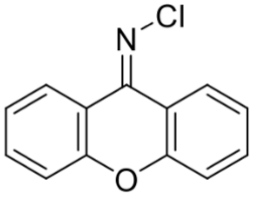

2c

168 mg, 73% yield, white solid.

^{1}H NMR (400 MHz, $CDCl_3$) δ 9.21 (dd, *J* = 1.2, 8.0 Hz, 1H), 8.15 (dd, *J* = 1.2, 8.0 Hz, 1H), 7.62 (ddd, *J* = 2.0, 7.2, 7.6 Hz, 1H), 7.54 (ddd, *J* = 1.6, 7.2, 7.2 Hz, 1H), 7.42 (dd, *J* = 1.2, 8.4 Hz, 1H), 7.34-7.29 (m, 2H), 7.29-7.24 (m, 1H).

^{13}C NMR (100.5 MHz, $CDCl_3$) δ 158.4, 153.8, 151.1, 133.2, 132.0, 129.2, 125.7, 124.1, 122.5, 121.3, 118.0, 117.2, 116.9.

IR (ATR) 3138, 1599, 1535, 1451, 1337, 1247, 767, 745 cm^{-1}.

HRMS (ESI) *m/z*: $[M+H]^+$ Calcd for $C_{13}H_8ONCl$ 230.0367; Found 230.0365.

(*E*)-*N*-chloro-3,4-dihydronaphthalen-1(2*H*)-imine

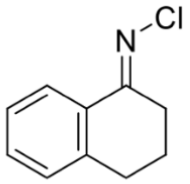

2d

339 mg, 88% yield, green oil.

^{1}H NMR (400 MHz, $CDCl_3$) δ 8.04 (d, *J* = 7.6 Hz, 1H), 7.32 (ddd, *J* = 1.2, 7.2, 7.2 Hz, 1H), 7.20 (dd, *J* = 7.2, 7.2 Hz, 1H), 7.15 (d, *J* = 7.6 Hz, 1H), 2.92 (t, *J* = 6.8 Hz, 2H), 2,76 (t, *J* = 6.0 Hz, 2H), 1.92 (tt, *J* = 6.0, 6.8 Hz, 2H).

^{13}C NMR (100.5 MHz, $CDCl_3$) δ 175.1, 140.4, 131.5, 130.9, 128.4, 126.5, 125.6, 31.9, 29.5, 21.8.

IR (ATR) 3066, 2938, 1609, 1578, 1556, 1450, 1437, 1295, 759, 730, 692 cm^{-1}.

HRMS (ESI) *m/z*: $[M+H]^+$ Calcd for $C_{10}H_{11}NCl$ 180.0575; Found 180.0574.

***N*-chloro-1,1-diphenylmethanimine**

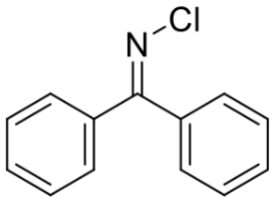

2e

350.5 mg, 76% yield, yellow oil.

^{1}H NMR (400 MHz, $CDCl_3$) δ 7.55-7.53 (m, 2H), 7.49-7.41 (m, 4H), 7.37-7.28 (m, 4H).

^{13}C NMR (100.5 MHz, $CDCl_3$) δ 178.5, 136.8, 136.2, 131.2, 129.6, 128.8, 128.4, 127.7.

IR (ATR) 3060, 1554, 1490, 1444, 1289, 1157, 1074, 1031, 955, 777, 736, 689, 617 cm^{-1}.

HRMS (ESI) *m/z*: $[M+H]^+$ Calcd for $C_{13}H_{11}NCl$ 216.0575; Found 216.0574.

(*E*)-*N*-chloro-1-phenylethan-1-imine

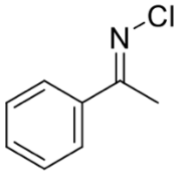

2f

290.3 mg, 88% yield, yellow oil.

^{1}H NMR (400 MHz, $CDCl_3$) δ 7.67-7.63 (m, 2H), 7.43-7.32 (m, 3H), 2.52 (s, 3H).

^{13}C NMR (100.5 MHz, $CDCl_3$) δ 176.9, 136.9, 130.6, 128.4, 126.7, 20.4.

IR (ATR) 1444, 1366, 1284, 1159, 1135, 1001, 762, 689 cm^{-1}.

HRMS (ESI) *m/z*: $[M+H]^+$ Calcd for C_8H_9NCl 154.0418; Found 154.0418.

Characterization of Products

1-((2-chloro-1,1-diphenylethyl)-λ4-azaneyl)-2,2,2-trifluoroethan-1-one

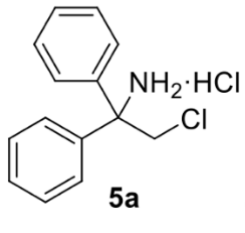

5a

55.1 mg, 68% yield, pale brown solid.
^{1}H NMR (400 MHz, CD_3OD) δ 7.52-7.43 (m, 6H), 7.39-7.34 (m, 4H), 4.57 (s, 2H).
^{13}C NMR (100.5 MHz, CD_3OD) δ 139.4, 130.3, 130.2, 128.0, 66.6, 49.9.
IR (ATR) 2862, 2138, 1598, 1519, 1449, 1403, 1028, 751, 726, 692 cm^{-1}.
HRMS (EI-TOF) *m/z*: $[M]^+$ Calcd for $C_{20}H_{16}O_3S$ 336.0820; Found 336.0834.
63.5 mg, 57% yield, pale yellow oil.

1-((2-chloro-1,1-di-*p*-tolylethyl)-λ4-azaneyl)-2,2,2-trifluoroethan-1-one

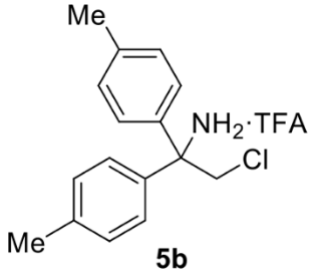

5b

^{1}H NMR (400 MHz, CD_3OD) δ 7.28 (d, *J* = 8.4 Hz, 4H), 7.20 (d, J = 8.4Hz, 4H), 4.49 (s, 2H), 2.37(s, 6H).
^{13}C NMR (100.5 MHz, CD_3OD) δ 140.5, 136.6, 130.7, 127.8, 66.2, 50.0, 21.0.
IR (ATR) 2865, 2138, 1598, 1518, 1500, 1449, 1405, 751, 727, 692, 624 cm^{-1}.
HRMS (ESI) *m/z*: $[M-CF_3CO_2H+Na]^+$ Calcd for $C_{16}H_{18}O_2NClNa$ 282.1020; Found 282.1013.

1-((2-chloro-1,1-bis(4-methoxyphenyl)ethyl)-λ4-azaneyl)-2,2,2-trifluoroethan-1-one

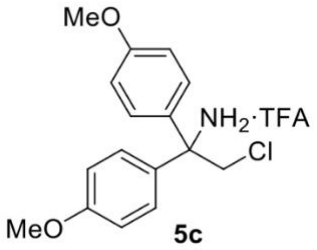

5c

12.8 mg, 11% yield, white solid.

^{1}H NMR (400 MHz, CD_3OD) δ 7.26-7.22 (m, 4H), 7.03-6.98 (m, 4H), 4.46 (s, 2H), 3.82(s, 6H).

^{13}C NMR (100.5 MHz, CD_3OD) δ 161.6, 131.4, 129.3, 115.4, 65.9, 55.9, 50.2.

IR (ATR) 2868, 2112, 1740, 1518, 1450, 1046, 694, cm^{-1}.

HRMS (ESI) *m/z*: $[M\text{-}CF_3CO_2]^+$ Calcd for $C_{16}H_{19}O_2NCl$ 292.1099; Found 170.0729.

1-((2-chloro-1,1-bis(4-chlorophenyl)ethyl)-λ4-azaneyl)-2,2,2-trifluoroethan-1-one

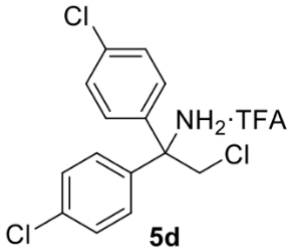

5d

68.3 mg, 55% yield, yellow oil.

^{1}H NMR (400 MHz, CD_3OD) δ 7.53 (d, *J* = 7.6 Hz, 4H), 7.36-7.32 (m, 4H), 4.55 (s, 2H).

^{13}C NMR (100.5 MHz, CD_3OD) δ 137.8, 136.6, 130.7, 130.4, 130.2, 130.1, 129.8, 65.9, 49.6.

IR (ATR) 2971, 1659, 1497, 1406, 1188, 1141, 1097, 1013, 821, 757, 720 cm^{-1}.

HRMS (EI-TOF) *m/z*: $[M]^+$ Calcd for $C_{20}H_{16}O_3S$ 336.0820; Found 336.0834.

1-((2-chloro-1,1-bis(4-fluorophenyl)ethyl)-λ4-azaneyl)-2,2,2-trifluoroethan-1-one

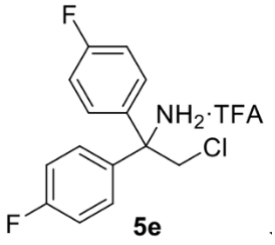

5e

82.0 mg, 72% yield, brown oil.

^{1}H NMR (400 MHz, CD_3OD) δ 7.42-7.39 (m, 4H), 7.28-7.20 (m, 4H), 4.56 (s, 2H).

^{13}C NMR (100.5 MHz, CD_3OD) δ 164.3 (d, $^1J_{F\text{-}C}$ = 248 Hz), 135.4 (d, $^4J_{F\text{-}C}$ = 3.8 Hz), 130.4 (d, $^3J_{F\text{-}C}$ = 8.6 Hz), 117.1 (d, $^2J_{F\text{-}C}$ = 22 Hz), 65.8, 49.9.

IR (ATR) 2971, 1659, 1604, 1511, 1435, 1242, 1171, 1138, 1046, 833, 800, 721, cm^{-1}.

HRMS (EI-TOF) *m/z*: $[M]^+$ Calcd for $C_{20}H_{16}O_3S$ 336.0820; Found 336.0834.

1-((1-chloro-2-phenylpropan-2-yl)-λ4-azaneyl)-2,2,2-trifluoroethan-1-one

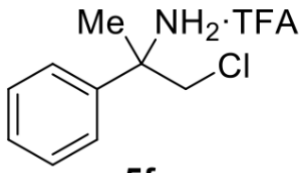

5f

37.0 mg, 43% yield, transparent oil.

^{1}H NMR (400 MHz, CD_3OD) δ 7.54-7.43 (m, 5H), 4.10 (d, *J* = 12.4 Hz, 1H), 3.98 (d, *J* = 12.4 Hz, 1H), 1.83 (s, 3H).

^{13}C NMR (100.5 MHz, CD_3OD) δ 139.4, 130.4, 130.2, 126.2, 60.6, 51.7, 24.0.

IR (ATR) 2989, 2222, 1662, 1388, 1432, 1182, 1134, 1026, 976, 837, 799, 767, 722, 696, cm^{-1}.

HRMS (ESI) *m/z*: $[M\text{-}CF_3CO_2]^+$ Calcd for $C_9H_{13}NCl$ 170.0731; Found 170.0729.

1-((2-chloro-1-phenylethyl)-λ4-azaneyl)-2,2,2-trifluoroethan-1-one

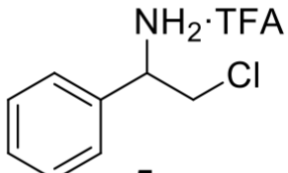

5g

20.8 mg, 26% yield, white solid.

^{1}H NMR (400 MHz, CD_3OD) δ 7.52-7.46 (m, 5H), 4.68 (dd, *J* = 5.2, 8.4 Hz, 1H), 4.05-3.96 (m, 2H).

^{13}C NMR (100.5 MHz, CD_3OD) δ 135.6, 130.9, 130.5, 128.2, 57.5, 46.2.

IR (ATR) 2959, 2177, 1515, 1362, 1108, 837, 761, cm^{-1}.
HRMS (ESI) *m/z*: $[M\text{-}CF_3CO_2]^+$ Calcd for $C_8H_{11}NCl$ 156.0575; Found 156.0573.

1-((1-(4-(*tert*-butyl)phenyl)-2-chloroethyl)-λ4-azaneyl)-2,2,2-trifluoroethan-1-one

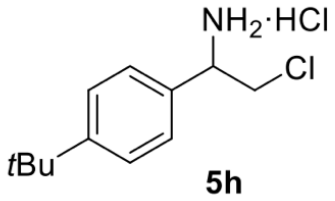

5h

23.5 mg, 42% yield, white solid.
^{1}H NMR (400 MHz, CD_3OD) δ 7.55-7.51 (m, 2H), 7.42-7.38 (m, 2H), 4.64 (dd, *J* = 5.6, 7.6 Hz, 1H), 4.04-3.94 (m, 2H).
^{13}C NMR (100.5 MHz, CD_3OD) δ 154.2, 132.6, 128.1, 127.4, 57.3, 46.3, 35.6, 31.6.
IR (ATR) 2959, 2617, 2177, 1515, 1362, 1016, 837, 761, cm^{-1}.
HRMS (ESI) *m/z*: $[M\text{-}Cl]^+$ Calcd for $C_{12}H_{19}NCl$ 212.1201; Found 212.1197.

1-((2-chloro-1-(4-methoxyphenyl)ethyl)-λ4-azaneyl)-2,2,2-trifluoroethan-1-one

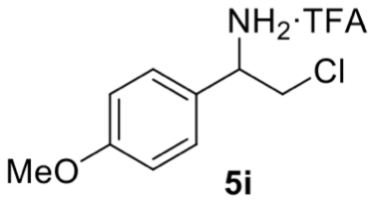

5i

27.1 mg, 30% yield, white solid.
^{1}H NMR (400 MHz, CD_3OD) δ 7.39 (d, *J* = 8.8 Hz, 2H), 7.02 (d, *J* = 8.8 Hz, 2H), 4.60 (t, *J* = 6.8 Hz, 1H), 3.97 (d, *J* = 6.8 Hz, 2H), 3.82 (s, 3H).
^{13}C NMR (100.5 MHz, CD_3OD) δ 162.2, 129.7, 127.4, 115.7, 57.1, 55.9, 46.2.
IR (ATR) 2959, 2617, 2177, 1515, 1362, 1015, 837, 760, cm^{-1}.
HRMS (ESI) *m/z*: $[M\text{-}CF_3CO_2]^+$ Calcd for $C_9H_{13}ONCl$ 186.0680; Found 186.0678.

1-((2-chloro-1-(4-chlorophenyl)ethyl)-λ4-azaneyl)-2,2,2-trifluoroethan-1-one

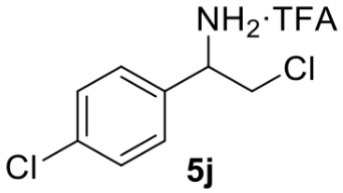

5j

31.1mg, 34% yield, white solid.

^{1}H NMR (400 MHz, CD_3OD) δ 7.53-7.45 (m, 4H), 4.73-4.69 (m, 1H), 4.05-3.94 (m, 2H).

^{13}C NMR (100.5 MHz, CD_3OD) δ 136.8, 134.3, 130.5, 130.1, 56.7, 46.0.

IR (ATR) 2959, 2617, 2177, 1515, 1362, 1015, 837, 760, cm^{-1}.

HRMS (ESI) *m/z*: $[M\text{-}CF_3CO_2]^+$ Calcd for $C_8H_{10}NCl_2$ 190.0185; Found 190.0183.

1-((1-([1,1'-biphenyl]-4-yl)-2-chloroethyl)-λ4-azaneyl)-2,2,2-trifluoroethan-1-one

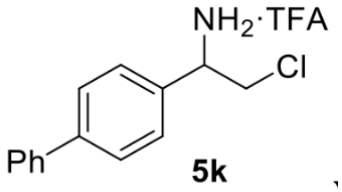

5k

30.5 mg, 29% yield, white solid.

^{1}H NMR (400 MHz, CD_3OD) δ 7.76 (d, *J* = 8.0 Hz, 2H), 7.65-7.62 (m, 2H), 7.56 (d, *J* = 8.0 Hz, 2H), 7.48 (t, *J* = 7.6 Hz, 2H), 7.40-7.35 (m, 1H), 4.73 (dd, *J* = 5.2, 7.6 Hz, 1H), 4.09-4.00 (m, 2H).

^{13}C NMR (100.5 MHz, CD_3OD) δ 144.0, 141.2, 134.4, 130.0, 129.0, 128.9, 128.8, 128.0, 57.2, 46.2.

IR (ATR) 2972, 1665, 1432, 1197, 1179, 1137, 1077, 837, 801, 751, 721, 698 cm^{-1}.

HRMS (ESI) *m/z*: $[M\text{-}CF_3CO_2]^+$ Calcd for $C_{14}H_{15}NCl$ 232.0888; Found 232.0883.

1-((2-chloro-1-(4-(chloromethyl)phenyl)ethyl)-λ4-azaneyl)-2,2,2-trifluoroethan-1-one

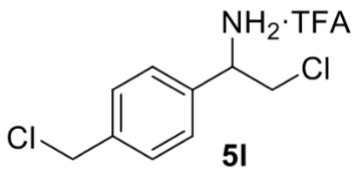

5l

32.4 mg, 34% yield, yellow oil.

^{1}H NMR (400 MHz, CD_3OD) δ 7.54 (d, *J* = 8.4 Hz, 2H), 7.47 (d, *J* = 8.4 Hz, 2H), 4.72 (dd, *J* = 5.2, 8.4 Hz, 1H), 4.68 (s, 2H), 4.05-3.95 (m, 2H).

^{13}C NMR (100.5 MHz, CD_3OD) δ 141.2, 135.6, 130.7, 128.7, 57.1, 46.1, 46.0.

IR (ATR) 2967, 2187, 1664, 1428, 1183, 1135, 1017, 838, 798, 722, 678 cm^{-1}.

HRMS (EI-TOF) *m/z*: $[M]^+$ Calcd for $C_{20}H_{16}O_3S$ 336.0820; Found 336.0834.

1-((2-chloro-1-(2-methoxyphenyl)ethyl)-λ4-azaneyl)-2,2,2-trifluoroethan-1-one

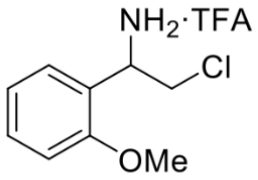

5m

16.0 mg, 18% yield, transparent oil.

^{1}H NMR (400 MHz, CD_3OD) δ 7.45 (dd, *J* = 7.6, 8.0 Hz, 1H), 7.35 (d, *J* = 8.0 Hz, 1H), 7.13 (d, *J* = 8.0 Hz, 1H), 7.05 (dd, *J* = 7.6, 8.0 Hz, 1H), 4.78 (dd, *J* = 4.4, 8.4 Hz, 1H), 4.07 (dd, *J* = 4.4, 8.4 Hz, 1H), 3.96 (dd, *J* = 4.4, 12 Hz, 1H), 3.92 (s, 3H).

^{13}C NMR (100.5 MHz, CD_3OD) δ 158.4, 132.5, 129.6, 122.8, 122.2, 112.7, 56.2, 54.5, 44.9.

IR (ATR) 2971, 1666, 1604, 1498, 1434, 1179, 1135, 1024, 837, 780, 754, 721 cm^{-1}.

HRMS (ESI) *m/z*: $[M\text{-}CF_3CO_2]^+$ Calcd for $C_9H_{13}ONCl$ 186.0680; Found 186.0678.

33.2 mg, 39% yield, white solid.

1-((2-chloro-1-phenylpropyl)-λ^4-azaneyl)-2,2,2-trifluoroethan-1-one

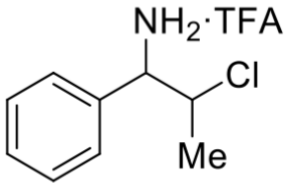

5n

^{1}H NMR (400 MHz, CD_3OD) δ 7.53-7.45 (m, 5H), 4.68 (major: d, *J* = 4.4 Hz, 0.86H), 4.66-4.58 (major: m, 0.86H), 4.55-4.47 (minor: m, 0.14H), 4.39 (minor: d, *J* = 10.6 Hz, 0.14H), 1.42 (major: d, *J* = 7.2 Hz, 2.57H), 1.37 (minor: d, *J* = 6.4 Hz, 0.43H).

^{13}C NMR (100.5 MHz, CD_3OD) All detected peaks were shown: δ 135.7, 133.7, 131.2, 130.8, 130.7, 129.9, 129.6, 128.7, 63.1, 60.6, 59.3, 58.8, 22.6, 21.7.
IR (ATR) 2988, 1661, 1522, 1185, 1139, 1064, 842, 723, 694 cm^{-1}.
HRMS (ESI) *m/z*: $[M\text{-}CF_3CO_2]^+$ Calcd for $C_9H_{13}NCl$ 170.0731; Found 170.0730.

1-((2-chloro-1,2-diphenylethyl)-λ4-azaneyl)-2,2,2-trifluoroethan-1-one

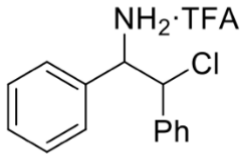

5o

From *trans*-stilbene 36.5 mg, 35% yield; from *cis*-stilbene 35.8 mg, 35% yield, white solid.
^{1}H NMR (400 MHz, CD_3OD) δ 7.49-7.20 (m, 10H), 5.52 (major: dd, *J* = 1.6, 6.4 Hz, 0.81H), 5.40 (minor: dd, *J* = 1.6, 10.4 Hz, 0.19H).
^{13}C NMR (100.5 MHz, CD_3OD) All detected peaks were shown: δ 138.1, 137.3, 135.1, 134.2, 130.8, 130.7, 130.6, 130.2, 129.9, 129.8, 129.6, 129.1, 129.0, 128.9, 65.1, 64.2, 62.5, 61.6.
IR (ATR) 2989, 1651, 1185, 1147, 801, 720, 695 cm^{-1}.
HRMS (ESI) *m/z*: $[M\text{-}CF_3CO_2]^+$ Calcd for $C_{14}H_{15}NCl$ 232.0888; Found 232.0884.

1-((2-chloro-2,3-dihydro-1*H*-inden-1-yl)-λ4-azaneyl)-2,2,2-trifluoroethan-1-one

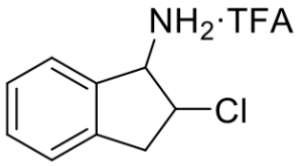

5p

27.9 mg, 33% yield, white solid.
^{1}H NMR (400 MHz, CD_3OD) δ 7.51 (d, *J* = 8.0 Hz, 1H), 7.45-7.35 (m, 3H), 5.06-5.00 (minor: m, 0.06H), 4.96 (minor: d, *J* = 6.0 Hz, 0.06H), 4.87 (major: d, *J* = 5.6 Hz, 0.94H), 4.65-4.59 (major: m, 0.94H), 3.75 (major: dd, *J* = 7.2, 16.8 Hz, 0.94H), 3.58 (minor: dd, *J* = 6.0, 17.2 Hz, 0.06H), 3.34 (minor: dd, *J* = 4.0, 17.2 Hz, 0.06H), 3.25 (major: dd, *J* = 6.0, 16.8 Hz, 0.94H).
^{13}C NMR (100.5 MHz, CD_3OD) All detected peaks were shown: δ 141.7, 136.9, 131.4, 129.1, 126.4, 125.4, 64.8, 60.4, 42.0.

IR (ATR) 2972, 2162, 1685, 1660, 1436, 1208, 1185, 1025, 836, 803, 746, 720 cm^{-1}.
HRMS (EI-TOF) *m/z*: $[M]^+$ Calcd for $C_{20}H_{16}O_3S$ 336.0820; Found 336.0834.

Transformations of Aminochlorination Products

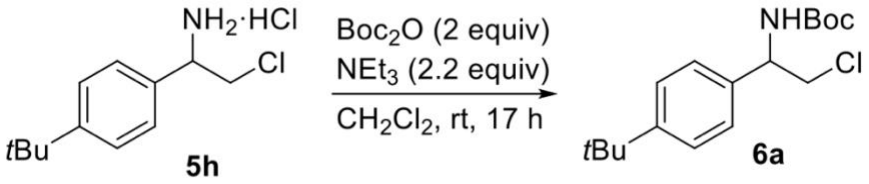

To a solution of **5h** (49.6 mg, 0.2 mmol) in DCM (1 mL) was added di-*tert*-butyl dicarbonate (87.3 mg, 0.4 mmol, 2 equiv) and triethylamine (63 μL, 2.2 equiv) at room temperature. After stirring for 17 h, the mixture was cooled to 0°C then washed with ice cold 0.5% HCl aq. EtOAc was added, and the organic layer was separated. The aqueous phase was extracted with EtOAc, and the combined organic layers were dried over Na_2SO_4, filtered and concentrated under reduced pressure. The residue was purified by column chromatography (Silica gel with EtOAc/Hexane 10%~50%) to afford **6a** as a pale yellow solid (46 mg, 72% yield).

^{1}H NMR (400 MHz, $CDCl_3$) δ 7.40-7.35 (m, 2H), 7.25-7.21 (m, 2H), 5.13 (brs, 1H), 4.99 (brs, 1H), 3.89-3.76 (m, 2H), 1.43 (brs, 9H), 1.31 (s, 9H).

^{13}C NMR (100.5 MHz, $CDCl_3$) δ 155.0, 150.9, 135.9, 126.2, 125.6, 80.0, 54.8, 48.1, 34.5, 31.3, 28.3.

IR (ATR) 3337, 2962, 1685, 1526, 1364, 1268, 1172, 1046, 1027, 824, 782, 762, 726, 682 cm^{-1}.

HRMS (ESI) *m/z*: $[M+Na]^+$ Calcd for $C_{17}H_{26}O_2NClNa$ 334.1544; Found 334.1540.

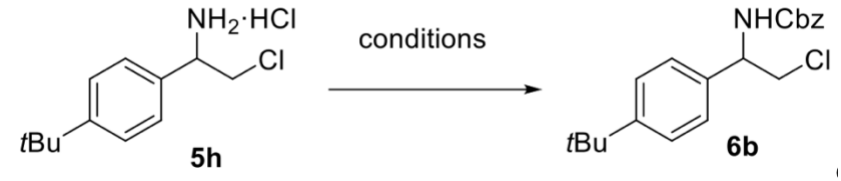

To a solution of **5h** (49.6 mg, 0.2 mmol) in THF (1 mL) was added benzyl chloroformate (62.2 μL , 0.4 mmol) and sodium bicarbonate (36.7 mg , 2 equiv) at 0°C. After stirring for 15min , EtOAc was added, and the organic layer was separated. The aqueous phase was extracted with EtOAc, and the combined organic layers were dried over Na_2SO_4, filtered and concentrated under reduced pressure. The residue was purified by column chromatography (Silica gel with EtOAc/Hexane 10%~50%) to afford **6b** as a white solid (38.1 mg, 55% yield) .

^{1}H NMR (400 MHz, $CDCl_3$) δ7.40-7.29 (m, 7H), 7.23 (d, *J* = 8.4 Hz, 2H), 5.39 (brs, 1H), 5.14 (d, *J* = 12 Hz, 1H), 5.09 (d, *J* = 12 Hz, 1H), 5.06 (brs, 1H), 3.89-3.75 (m, 2H), 1.31 (s, 9H).

^{13}C NMR (100.5 MHz, CD_3CN) δ 156.8, 151.8, 138.1, 137.7, 129.4, 128.8, 128.6, 127.4, 126.5, 118.3, 67.0, 57.2, 48.3, 35.1, 31.4.

IR (ATR) 3291, 2965, 1684, 1532, 1262, 1220, 1046, 825, 782, 761, 732, 693, 681 cm^{-1}.

HRMS (ESI) *m/z*: $[M+H]^+$ Calcd for $C_{20}H_{25}O_2NCl$ 346.1568; Found 346.1563.

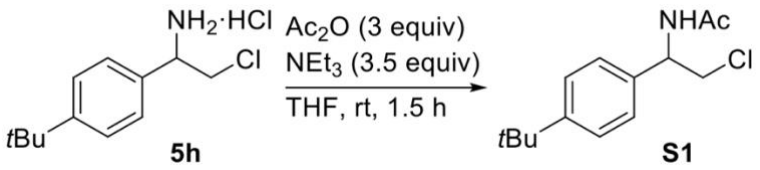

To a solution of **5h** (70 mg, 0.28 mmol) in THF (1 mL) was added acetic anhydride (79.4 μL, 3 equiv) and triethylamine (0.14 mL, 3.5 equiv) were added dropwise at room temperature. After stirring for 1.5 h, 1M HCl aq and EtOAc were added subsequently, and the organic layer was separated. The aqueous phase was extracted with EtOAc, and the combined organic layers were dried over Na_2SO_4, filtered and concentrated under reduced pressure. The residue was purified by column chromatography (Silica gel with EtOAc/Hexane 10%~50%) to afford **S1** as a white solid (53 mg, 74% yield).

^{1}H NMR (400 MHz, $CDCl_3$) δ 7.38 (d, *J* = 8.0 Hz, 2H), 7.24 (d, *J* = 8.0 Hz, 2H), 6.16 (d, *J* = 8.0 Hz, 1H), 5.36-5.29 (m, 1H), 3.87 (dd, *J* = 5.6, 11.6 Hz, 1H), 3.83 (dd, *J* = 5.6, 11.6 Hz, 1H), 2.04 (s, 3H), 1.31 (s, 9H).

^{13}C NMR (100.5 MHz, $CDCl_3$) δ 169.6, 151.1, 135.3, 126.4, 125.7, 53.2, 47.4, 34.5, 31.2, 23.3.

IR (ATR) 3255, 2961, 1646, 1549, 1375, 1304, 1114, 1058, 1018, 823, 760, 728, 685 cm^{-1}.

HRMS (ESI) *m/z*: $[M+H]^+$ Calcd for $C_{14}H_{21}ONCl$ 254.1306; Found 254.1301.

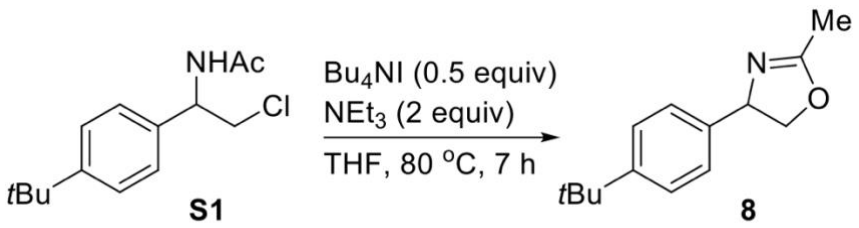

To a solution of **S1** (28.8 mg, 0.11 mmol) in THF (1 mL) were added tetra-n-butylammonium iodide (20.3 mg , 0.5 equiv) and triethylamine (30.6 μL, 2 equiv) at 80 °C . After stirring for 7h, EtOAc was added, and the organic layer was separated. The aqueous phase was extracted with EtOAc, and the combined organic layers were dried over Na_2SO_4, filtered and concentrated under reduced pressure. The residue was purified by column chromatography (Silica gel with EtOAc/Hexane 10%~50%) to afford the oxazoline **8** as a transparent oil (19 mg, 80% yield).

^{1}H NMR (400 MHz, $CDCl_3$) δ 7.39-7.34 (m, 2H), 7.21-7.17 (m, 2H), 5.14 (dd, *J* = 8.4, 10 Hz, 1H), 4.58 (dd, *J* = 8.0, 10 Hz, 1H), 4.13 (dd, *J* = 8.0, 8.4 Hz, 1H), 2.09 (d, *J* = 1.2 Hz, 3H), 1.31 (s, 9H).

^{13}C NMR (100.5 MHz, $CDCl_3$) δ 165.5, 150.4, 139.3, 126.2, 125.6, 74.5, 69.4, 34.5, 31.3, 29.7 , 13.9.

IR (ATR) 2960, 1743, 1668, 1549, 1512, 1387, 1364, 1269, 1228, 1109, 985, 828 cm^{-1}.

HRMS (ESI) *m/z*: $[M+H]^+$ Calcd for $C_{14}H_{20}ON$ 218.1539; Found 218.1536.

Single Crystal XRD Analysis of 2c

A suitable crystal was mounted with liquid paraffin on a MiTeGen MicroMounts and transferred to the goniometer in a nitrogen stream at 133 K. Measurement was made on a RIGAKU XtaLAB Synergy-DW system with 1.2 kW PhotonJet-DW microfocus rotating anode using graphite monochromated Cu-K_a radiation (λ = 1.54184 Å) and HyPix-6000HE detector. Cell parameters were determined and refined, and raw frame data were integrated using CrysAlis^{Pro} (Agilent Technologies, 2010). The structures were solved by direct methods with SHELXT[2] and refined by full-matrix least-squares techniques against F^2 with SHELXL-2018/3[3] by using Olex2 software package.[4] The non-hydrogen atoms were anisotropically refined, and hydrogen atoms were placed using AFIX instructions. Crystal data and structure refinement parameters are in Table S3. The Mercury program was used to draw the molecule structures in Figure 3.3.

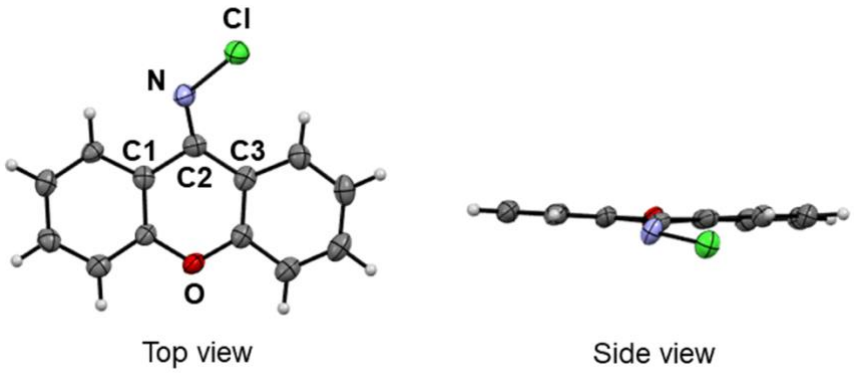

Figure 3.3 : ORTEP drawing of 2c showing 50% probability thermal ellipsoids. Selected bond lengths (Å) and angles (deg.) for 2c: N–Cl, 1.725(4); C2–N, 1.277(7); C1–C2–N, 112.5(5); C1–C2–C3, 114.2(4); C3–C2–N, 133.2(5); C2–N–Cl, 120.0(4).

empirical formula	$C_{26}H_{16}Cl_2N_2O_2$	D_{calcd}, g/cm^{-3}	1.511
CCDC number	2262168	μ[Cu-$K\alpha$], mm^{-1}	3.127
formula weight	459.31	T, K	133
crystal system	monoclinic	crystal size, mm	0.20 × 0.18 × 0.02
space group	Pc(#7)	θ range for data collection (deg.)	6.78 to 152.2
a, Å	13.3914(5)	no. of reflections measured	8684
b, Å	4.9489(2)	unique data ($Rint$)	3380 (0.0427)
c, Å	15.6475(7)	data/restraints/parameters	3380 / 2 / 289
α, deg.	90	$R1$ ($I > 2.0\sigma(I)$)	0.0481
β, deg.	103.217(4)	$wR2$ ($I > 2.0\sigma(I)$)	0.1347
γ, deg.	90	$R1$ (all data)	0.0534
V, Å^3	1009.53(7)	$wR2$ (all data)	0.1388
Z	2	GOF on F^2	1.076

$R1 = (\Sigma||Fo|-|Fc||)/(\Sigma|Fo|)$. $wR2 = [\{\Sigma w(Fo^2-Fc^2)^2\}]/(\Sigma w(Fo^4)\}]^{1/2}$.

Table 3.4: Crystal Data and Data Collection Parameters of **2c**.

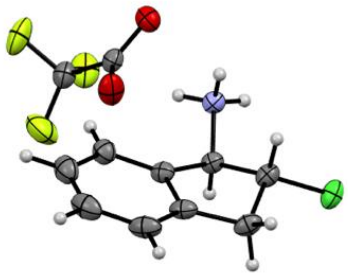

Figure S3. ORTEP drawing of **5p** showing 50% probability thermal ellipsoids.

empirical formula	$C_{11}H_{11}ClF_3NO_2$	D_{calcd}, g/cm^{-3}	1.544
CCDC number	2267189	m[Cu-Ka], mm^{-1}	3.141
formula weight	281.66	T, K	133
crystal system	monoclinic	crystal size, mm	0.2 × 0.03 × 0.02
space group	$P2_1/c$(#14)	q range for data collection (deg.)	7.912 to 153.392
a, Å	4.84570(10)	no. of reflections measured	24828
b, Å	22.3506(3)	unique data (Rint)	2516 (0.0718)
c, Å	11.3792(2)	data/restraints/parameters	2516 / 0 / 164
a, deg.	90	$R1$ ($I > 2.0s(I)$)	0.0462
b, deg.	100.628(2)	$wR2$ ($I > 2.0s(I)$)	0.1168
g, deg.	90	$R1$ (all data)	0.0513
V, Å^3	1211.27(4)	$wR2$ (all data)	0.1201
Z	4	GOF on F^2	1.063

$R1 = (S||Fo|-|Fc||)/(S|Fo|)$. $wR2 = [\{Sw(Fo^2-Fc^2)^2\}]/(Sw(Fo^4)\}]^{1/2}$.

Table 3.5: Crystal Data and Data Collection Parameters of **5p**

DFT Calculations

All geometry optimizations and frequency analyses were performed by Gaussian 16 C.01 package. The geometry optimizations of all structures were conducted at the UωB97X-D/6-31+G(d,p) level of theory with the solvation model (SMD: dichloromethane) and "guess=mix" keyword. Frequency analyses were performed at the same level of theory for geometry optimizations, in which the thermal free energy corrections were provided to determine the solution phase Gibbs free energies (ΔG_{sol}) at 298.15 K (25 °C). All the transition states have the single imaginary frequency, and all the optimized structures as minima have no imaginary frequency. The transition states were traced with intrinsic reaction coordinate (IRC) analyses to confirm the connection of the reaction pathway. For discussion, relative Gibbs free energies (ΔG_{sol}) were calculated from $\Delta G_{sol} = \Sigma G_{sol}$ (for products) – ΣG_{sol} (for reactants). A picture of 3D model for **TS** was described by using CYLview20.

Summary of Energies

Structure Name	spin	Electronic energy [Hartree]	Gibbs free energies [Hartree]	ν_{min} [cm^{-1}]
2a	singlet	-1014.958383	-1014.821798	66.14
2a*	triplet	-1014.886614	-1014.755322	61.46
TS	triplet	-1014.886283	-1014.755269	-296.76
A	doublet	-554.757743	-554.622855	96.02
B	doublet	-460.120761	-460.136438	N/A
1g	singlet	-309.570292	-309.466856	59.81
C	doublet	-769.741485	-769.639904	61.52
TS1	doublet	-864.315418	-864.057270	-497.76
D	doublet	-864.362003	-864.099783	12.24
3g	singlet	-1324.601311	-1324.335455	19.14
TS2	doublet	-1784.690463	-1784.429496	-554.69
E	doublet	-1784.723430	-1784.460128	21.09
F	doublet	-1784.718074	-1784.454664	21.55
TS2'	doublet	-1784.718071	-1784.453660	-53.93
TS3	doublet	-1784.685289	-1784.427473	-550.20
4g	singlet	-1229.972666	-1229.868393	40.94

Detailed Pathway for Forming 3g from Intermediate E

References

[1] Kerru, N.; Gummidi, L.; Maddila, S.; Gangu, K.K.; Jonnalagadda, S.B. *Molecules* **2020**, *25*, 1909.

[2] Legnani, L.; Prina-Cerai, G.; Delcaillau, T.; Willems, S.; Morandi, B. *Science* **2018**, *362*, 434−439.

[3] Li, Y.; Liang, Y.; Dong, J.; Deng, Y.; Zhao, C.; Su, Z.; Guan, W.; Bi, X.; Liu, Q.; Fu, J. *J. Am. Chem. Soc.* **2019**, *141*, 18475−18485.

[4] Gavaerts, S.; Angelini, L.; Hampton, C.; Malet-Sanz, L.; Ruffoni, A.; Leonori, D. *Angew. Chem. Int. Ed.* **2020**, *59*, 15021−15028.

[5] (a) Luca, L. D.; Giacomelli, G. *Synlett* **2004**, 2180−2184. (b) Qi, B.; Li, L.; Wang, Q.; Zhang, W.; Fang, L.; Zhu, J. *Org. Lett.* **2019**, *21*, 6860−6863.

[6]: (a) Kondo, Y.; Kadota, T.; Hirazawa, Y.; Morisaki, K.; Morimoto, H. Ohshima, T.. *Org. Lett.* **2020**, *22*, 120−125. (b) Kondo, Y.; Hirazawa, Y.; Kadota, T.; Yamada, K.; Morisaki, K.; Morimoto, H.; Ohshima, T. *Org. Lett.* **2022**, *24*, 6594−6598.

[7]: Cismesia, M. A.; Yoon, T. P. *Chem. Sci.* **2015**, *6*, 5426−5434.

[8]: Gaussian 16, Revision C.01, M. J. Frisch, G. W. Trucks, H. B. Schlegel, G. E. Scuseria, M. A. Robb, J. R. Cheeseman, G. Scalmani, V. Barone, G. A. Petersson, H. Nakatsuji, X. Li, M. Caricato, A. V. Marenich, J. Bloino, B. G. Janesko, R. Gomperts, B. Mennucci, H. P. Hratchian, J. V. Ortiz, A. F. Izmaylov, J. L. Sonnenberg, D. Williams-Young, F. Ding, F. Lipparini, F. Egidi, J. Goings, B. Peng, A. Petrone, T. Henderson, D. Ranasinghe, V. G. Zakrzewski, J. Gao, N. Rega, G. Zheng, W. Liang, M. Hada, M. Ehara, K. Toyota, R. Fukuda, J. Hasegawa, M. Ishida, T. Nakajima, Y. Honda, O. Kitao, H. Nakai, T. Vreven, K. Throssell, J. A. Montgomery, Jr., J. E. Peralta, F. Ogliaro, M. J. Bearpark, J. J. Heyd, E. N. Brothers, K. N. Kudin, V. N. Staroverov, T. A. Keith, R. Kobayashi, J. Normand, K. Raghavachari, A. P. Rendell, J. C. Burant, S. S. Iyengar, J. Tomasi, M. Cossi, J. M. Millam, M. Klene, C. Adamo, R. Cammi, J. W. Ochterski, R. L. Martin, K. Morokuma, O. Farkas, J. B. Foresman, and D. J. Fox, Gaussian, Inc., Wallin.

Publication List

Publications included in the thesis:

[1] Ryotaro Niizeki,Kosuke Higashida,**Emna Mejri**, Masaya Sawamura, Yohei Shimizu. Synthesis of C,N,N-Cyclometalated Gold(III) Complexes with Anionic Amide Ligands. *Synlett* **2021**. doi: 10.1055/a-1673-9236.

[2] **Emna Mejri**, Kosuke Higashida, Yuta Kondo, Anna Nawachi, Hiroyuki Morimoto, Takashi Ohshima,Masaya Sawamura, and Yohei Shimizu.Visible-Light-Induced Aminochlorination of Alkenes. *Org.Lett* **2023** (as soon as published). doi: 10.1021/acs.orglett.3c01645.

Acknowledgement

The research described in this thesis was carried out under the supervision of Prof. Dr. Masaya Sawamura at the Department of Chemistry (Faculty of Science), Hokkaido University from Nov. 2020 to Sept. 2023.

E. Mejri thanks Prof. Dr. Masaya Sawamura for kind supervision and meaningful discussions, which revealed the insight of the reaction nature and significantly improved the quality of research.

E. Mejri thanks Associate Professor Dr. Yohei Shimizu for advice, discussions, and supervision during the graduate school research. The part of computational studies in this thesis was carried out in collaboration with Assistant Professor Dr. Kosuke Higashida.

E. Mejri thanks him for his contributions and collaboration. E. Mejri appreciates Assistant Professor Yusuke Masuda, Assistant Professor Dr. Fernando Arteaga Arteaga and Associate Professor Dr. Dennis Chung-Yang Huang for meaningful discussions and assistance.

E. Mejri is grateful to examiners of her doctoral thesis. The insightful suggestions from Prof. Dr. Hajime Ito, Prof. Dr. Aiichiro Nagaki were meaningful for improving the quality of this thesis.

E. Mejri extends her heartfelt appreciation to the MEXT Doctoral program for their generous scholarship support, which has been instrumental in her academic pursuits.

She would also like to express deep gratitude to her beloved family, Mr. Belhay Mejri, Ms. Nejia Barhoumi, and her brother Hazem Mejri, for their unwavering support from her childhood through her graduate school studies. Their warmth and encouragement have been indispensable in enabling her to pursue her education far from home.

E. Mejri would like to thank Ms. Hamidah Hashim, Ms. Takumi Kimura, Mr. Masato Inoue, and Mr. Marwen Ben Hriz for their kind support and assistance throughout her entire graduate school journey. Their guidance has greatly contributed to her academic growth and achievements. Additionally, she acknowledges the other alumni, friends, and current members of the Organometallic Chemistry Laboratory, including Dr. Z. You, Dr. Y. Ueda, Ms. I. Qureshi, Ms. P. Saha, Ms. Y. Kawamura, Mr. S. Sakai, Mr. X. Liu, Mr. Y. Heike, for their invaluable contributions through discussions and collaborative efforts. Their collective involvement has enriched her research experience and fostered a collaborative environment.

Emna MEJRI
CSE, Hokkaido University
Sept. 2023